UNIVERSITY OF GENOVA

PHD PROGRAM IN BIOENGINEERING AND ROBOTICS

High Sensitivity, Label-Free, Interferometric Biosensor for In Vitro Contractility Assessment of HiPSC Cardiomyocytes

Alessio Boschi

Thesis submitted for the degree of Doctor of Philosophy (XXXVI◦ cycle)

Thesis Jury

Francesco Gentile

Laura Fabris

Supervisor

Francesco De Angelis

Head of PhD

Giorgio Cannata

UniGe | DIBRIS

Table of Contents

Summary

The exploration of in vitro cell cultures holds pivotal significance in biological studies, providing a crucial lens through which we examine cellular responses to external stimuli. This is especially pertinent in the field of cardiomyocytes contraction measurement, where the need for accurate and versatile methodologies persists. Past strategies have made strides, yet limitations persist, necessitating innovative solutions in the coming decade. As technology and biology converge, advancements are anticipated in fabrication techniques, sensing materials, and platform designs. The maturation of cardiomyocytes and optimization of culturing protocols promise to refine functional measurements, aligning them more closely with in vivo conditions. Micro- and nanoscale biomaterials have emerged as transformative agents, surmounting the constraints of previous technologies. They lay the groundwork for platforms that interface with electrogenic cells at unprecedented spatiotemporal scales, offering a holistic view of interactions among different cell and organ types.

The first chapter of this thesis describes the principal mechanisms governing cardiac tissue contraction, both in vivo and in vitro models. This foundational understanding sets the stage for delving into the challenges inherent in measuring cardiac tissues in vitro.

In the second chapter, a comprehensive review unfolds, surveying the current methods employed for measuring cardiomyocyte contraction across diverse biological models. From single-cell analyses to intricate 3D organoid models, a spectrum of approaches is scrutinized, highlighting the nuances and limitations of each.

The third chapter marks a pivotal turn, introducing a novel device designed for measuring the contraction force of a 2D monolayer of cardiomyocytes. This technological innovation stands as a testament to the evolving landscape of cardiac research tools.

The fourth chapter navigates the translation of this technology from whole cell culture to single-cell resolution.

1 Introduction to Cardiac Muscle Contraction

This chapter provides a comprehensive overview of the fundamental aspects of cardiac muscle contraction. It begins by exploring the anatomy and physiology of the heart, delving into the intricate structure of the human heart, including its chambers, valves, and the myocardium, which is the primary muscle tissue responsible for the heart's rhythmic contractions. The chapter also highlights the unique properties and characteristics of cardiac muscle tissue, emphasizing the specialized structure and function of cardiomyocytes, the primary cellular units of the myocardium. Furthermore, the chapter delves into the molecular and cellular processes that underlie cardiomyocyte contraction, focusing on the sliding filament model of muscle contraction. It elucidates the four key steps involved in the contraction cycle, including the binding of myosin to actin, the powerstroke, actin release, and ATP binding, which collectively lead to the shortening of sarcomeres and the generation of muscle contraction. Additionally, the chapter discusses the process of excitation-contraction coupling, detailing how the rise in cytosolic calcium levels triggers the interaction between actin and myosin, ultimately leading to cardiomyocyte contraction. Finally, the chapter provides an in-depth explanation of the electrical conduction system within the heart and its pivotal role in coordinating the rhythmic contractions of the atria and ventricles. It elucidates the sequential transmission of electrical signals from the sinoatrial node to the atrioventricular node, the bundle of His, and the Purkinje fibers, which collectively orchestrate the precise timing of atrial and ventricular excitation essential for optimal cardiac pump function. Overall, Chapter 1 serves as a foundational guide to understanding the intricate processes that govern cardiac muscle contraction, providing a comprehensive overview of the anatomical, physiological, and molecular aspects of this fundamental physiological mechanism. The detailed insights presented in this chapter lay the groundwork for the subsequent discussions on the application of nanotechnologies for in vitro cardiac contractility, which are covered in the subsequent chapters of the manuscript.

1.1 Fundaments of anatomy and physiology of the Heart

1.1.1 Overview of the heart's structure

The human heart, an intricately designed organ, orchestrates optimal blood circulation throughout the body. Its structure is a harmonious composition of interconnected chambers, valves, and blood vessels, all enveloped by a protective membrane known as the pericardium. The heart's exterior-to-interior composition features three distinct layers: the epicardium (outer layer), the myocardium (middle layer), and the endocardium (inner layer). Playing a crucial role in pumping blood, the myocardium, composed of cardiac muscle tissue, constitutes approximately 95% of the heart wall. The cardiac muscle fibers (cells) are organized in spiraling bundles, generating the powerful pumping actions. Despite exhibiting striation similar to skeletal muscle, the cardiac muscle functions involuntarily. Functioning as two separate pumps, the heart comprises the right heart, propelling blood through the lungs, and the left heart, circulating blood to peripheral organs. Each of these heart sections comprises an atrium and a ventricle, forming a pulsatile two-chamber pump. Regulating blood flow are valves constructed of dense connective tissue covered by endocardium. Blood flows from the right atrium to the right ventricle through the tricuspid valve, while the left atrium to the left ventricle passage occurs via the bicuspid (mitral) valve. Interconnected with a network of blood vessels, the heart maintains blood transport to and from various body parts. Notably, the aorta, the largest artery, conveys oxygenated blood from the left ventricle to systemic circulation, while the pulmonary artery conveys deoxygenated blood from the right ventricle to the lungs for oxygenation. To accomplish the intricate task of blood circulation, specialized mechanisms within the heart orchestrate a continuous sequence of heart contractions known as cardiac rhythmicity. These mechanisms transmit ionic signals (action potentials) throughout the cardiac muscle, culminating in the heart's rhythmic beating. The human heart functions as a syncytium of interconnected heart muscle cells, allowing action potentials to spread across cells, forming atrial and ventricular syncytia. These syncytia consist of different types of tissues, including atrial and ventricular muscle, as well as specialized excitatory and conductive muscle fibers. The atrial and ventricular muscle types contract similarly to skeletal muscle, with the distinction that their contractions last longer. Ordinarily, action potentials are not directly conducted between the atrial and ventricular syncytia through fibrous tissue. Instead, conduction

occurs via the specialized bundle of conductive fibers discussed further in Chapter 1.2.2. The ability to achieve synchronized and rhythmic contractions among numerous myocytes, precisely coordinated in sequence and timing, along with the capacity to modulate this mechanism in response to diverse physiological conditions, fundamentally contributes to maintaining human homeostasis[1,2].

1.1.2 Description of the cardiac muscle tissue's unique properties and characteristics

The myocardium, the main muscle tissue, is a specialized flesh that constitutes the middle layer and bulk of the heart wall. It possesses unique structural, functional, and electrochemical properties that enable the continuous, synchronous, and rhythmic contractions required to pump blood throughout the body[3]. The main cellular unit of cardiac muscle tissue is the cardiomyocyte, which are cylindrical, branched, and striated muscle cells. Cardiomyocytes are typically 100-150 μm long and 10-25 μm wide in humans[4]. A unique feature of cardiac muscle, unlike skeletal muscle, is the presence of so called “intercalated discs”, transversal structures that electrically and mechanically connect cardiomyocytes end-to-end, ensuring rapid action potential propagation[5]. The building block of cardiomyocytes, its contractile unit, it is called sarcomere. Sarcomeres are composed of thin filaments made of actin and thick filaments of myosin, which, thanks to a complex biochemical cascade process, slide past each other to produce contraction [6]. Finally, two important components of cardiomyocytes are the sarcoplasmic reticulum and T-tubules. The sarcoplasmic reticulum is a network of vesicles that store and release Ca^{2+} ions, which are pivotal for initiating the sliding of actin and myosin filaments during contraction. The sarcoplasmic reticulum surrounds each myofibril and releases Ca^{2+} to trigger contraction in response to electrical stimulation.

In addition to contractile cardiomyocytes, cardiac muscle contains other specialized cell types, including:

- Pacemaker cells in the sinoatrial node - These cells can self-excite due to funny channel proteins like HCN4, initiating impulses that spread through the heart, controlling the rhythmic beating rate[7].

- Conducting cells in the atrioventricular node, bundle of His, and Purkinje fibers - These cells lack contractile elements but rapidly propagate action potentials via gap junctions between cells.

- Fibroblasts – These produce extracellular matrix components like collagen that provide structural support and coordinate mechanical force transmission[8].

- Endothelial and smooth muscle cells – These line coronary blood vessels that perfuse the myocardium[9].

1.2 Cardiomyocyte Structure and Function

1.2.1 Cardiomyocyte structure, including sarcomeres, myofibrils, and ion channels

The sarcolemma is the plasma membrane of cardiomyocytes. It contains pivotal invaginations called transverse tubules (T-tubules) which first aim is the rapid propagation of Ca2+ ions from the outside to inside of the cell, ensuring the action potentials traveling on the sarcolemma can deep into the cell interior[10,11]. Within the sarcolemma lies the sarcoplasm, the cytoplasm of cardiomyocytes. The sarcoplasm contains glycogen that can be broken down to synthesize ATP. It also contains the oxygen-binding protein myoglobin that facilitates oxygen delivery to mitochondria[12]. Mitochondria lie between myofibrils in rows, strategically positioned to provide ATP where needed for muscle contraction. Their proximity to the contractile elements allows rapid ATP production to power contraction. Other sarcoplasmic organelles include the sarcoplasmic reticulum which stores and releases Ca2+ ions to initiate contraction[13]. The sarcoplasmic reticulum (SR) is an elaborate network of membranous sacs that surrounds each myofibril. It functions to store and release Ca2+ ions needed to trigger muscle contraction. Enlarged terminal cisternae portions of the SR are closely associated with T-tubules in specialized triad junctions[13,14]. When an action potential travels into the cardiomyocyte via the T-tubules, it stimulates the release of Ca2+ from the SR terminal cisternae. The sudden increase in local Ca2+ then initiates crossbridge cycling and contraction of the adjacent sarcomeres in each myofibril. This intimate relationship

between T-tubules and SR facilitates rapid propagation of electrical signals into the cell interior and synchronous Ca2+ release throughout the cardiomyocyte to trigger coordinated contraction[15].

The most important components of a skeletal muscle are the muscle fibers themselves. Within myofibrils are thin actin filaments and thick myosin filaments. The filaments are organized into compartments called sarcomeres, which are the functional units of contraction[6,16]. Sarcomeres are delimited by Z discs, with a sarcomere extending from one Z disc to the next. The A band is the dark central region of a sarcomere where thin and thick filaments overlap. The lighter I band on either side contains just thin filaments[16]. The H zone in the center of the A band contains only thick filaments. The alternating pattern of light I bands and dark A bands generates the striated appearance of myofibrils and whole muscle fibers. The M line in the H zone contains proteins that anchor thick filaments at their midpoint. This highly ordered arrangement of overlapping protein filaments enables the coordinated contraction of sarcomeres in myofibrils to generate force in cardiomyocytes[17]. Here is an expanded description of key sarcolemmal ion channels and transporters in cardiomyocytes:

- Voltage-gated sodium channels (NaV1.5) are responsible for the rapid upstroke (depolarization) phase of the cardiac action potential. These channels rapidly open when the membrane potential becomes slightly positive, allowing inward flux of sodium ions that further depolarizes the membrane. This activates adjacent voltage-gated sodium channels, propagating the action potential.

- L-type calcium channels (CaV1.2) activate more slowly than sodium channels, opening in response to stronger depolarization. This allows calcium influx, which initiates excitation-contraction coupling by triggering calcium release from the sarcoplasmic reticulum. L-type calcium channels play a key role in regulating intracellular calcium and contractility.

- Voltage-gated potassium channels (KV11.1, KV7.1) open in response to depolarization, allowing efflux of potassium ions down their concentration gradient. Different potassium channels activate with varied kinetics, contributing to repolarization of the cardiomyocyte membrane potential. This shapes the cardiac action potential waveform.

- Voltage-gated chloride channels help set the resting membrane potential of cardiomyocytes closer to the chloride equilibrium potential, making it more negative. Chloride influx upon opening opposes depolarization.

- The sodium-calcium exchanger (NCX) utilizes the electrochemical gradient of sodium to pump calcium ions out of the cell. This returns intracellular calcium to normal low levels following contraction. The exchanger moves 3 sodium ions into the cell in exchange for pumping out 1 calcium ion.

- The sodium-potassium ATPase pump consumes ATP to actively transport 3 sodium ions out and 2 potassium ions into the cell against their concentration gradients. This maintains the sodium and potassium gradients crucial for generating action potentials and muscle contraction.

1.2.2 Explanation of the electrical conduction system within the heart and its role in coordinating contractions

The cardiac conduction system utilizes specialized cells to generate and conduct action potentials, enabling contraction of the heart. This contraction signal initiates in the sinoatrial node, located in the upper right atrium, which contains pacemaker cells that spontaneously depolarize to generate an action potential due to increased permeability to Na+ and Ca2+ ions[7]. This impulse spreads rapidly through both atria via internodal pathways, composed of ordinary working cardiomyocytes, but with more gap junctions and faster conduction velocity. Upon reaching the atrioventricular node (AV node), conduction slows due to smaller, fewer gap junctions, creating a delay that allows complete atrial contraction before ventricular activation[7,18]. From the AV node, the signal enters the only electrical connection between atria and ventricles - the bundle of His. The bundle of His contains specialized cardiac fibers lacking contractile machinery but exhibiting rapid conduction via abundant gap junctions. The bundle of His bifurcates into right and left bundle branches descending through the interventricular septum. The bundle branches further divide into a network of Purkinje fibers, which are rapidly conducting cells with fewer myofibrils. The Purkinje fibers rapidly propagate the impulse to the apex of the heart, stimulating coordinated ventricular contraction via the ventricular conduction network. This specialized conduction system

coordinates the precise timing of atrial and ventricular excitation needed for optimal cardiac pump function. Disruptions can lead to arrhythmias[7,9,19].

1.3 Mechanism of Contraction

1.3.1 Molecular and cellular processes of cardiomyocyte contraction

The contraction cycle in cardiomyocytes relies on the sliding filament model of muscle contraction and involves four key steps:

1) *Binding of myosin to actin* - The rise in cytosolic Ca2+ levels causes Ca2+ to bind troponin C, shifting the tropomyosin complex and exposing myosin binding sites on actin filaments. The myosin head domains can then bind to these sites on actin to form crossbridges.

2) *Powerstroke* - The myosin heads tilt to produce a powerstroke upon ATP hydrolysis, pulling the actin filaments toward the center of the sarcomere.

3) *Actin release* - After the powerstroke, ADP and inorganic phosphate are released, causing a conformational change in myosin that results in detachment of actin.

4) *ATP binding* - Binding of a new ATP molecule to myosin causes it to dissociate from actin and recock the myosin head back into a high energy position.

The cyclical repetition of these steps - crossbridge formation, powerstroke, actin release, and ATP binding - causes the thin filaments to slide inward past the thick filaments. This shortens the sarcomere and produces muscle contraction.

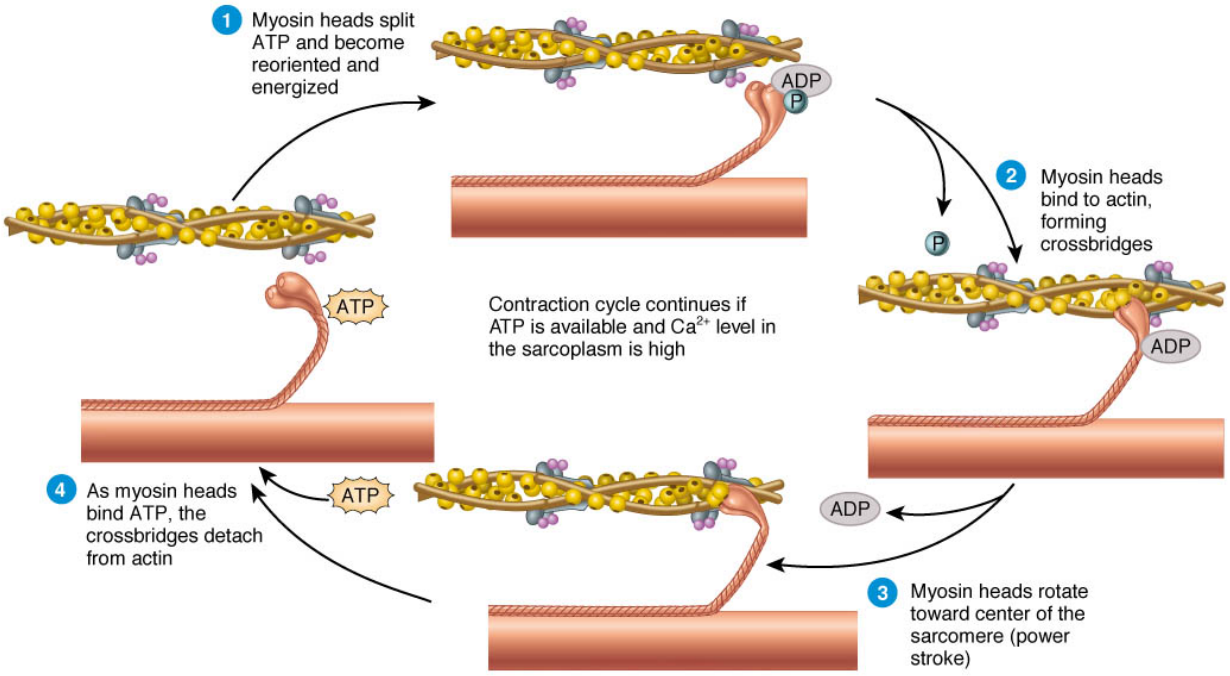

Figure 1.1 schematic representation of the molecular process leading to fiber contraction and force generation. Image from mykindofscience.com.

The process that leads cardiomyocytes to contract is called excitation-contraction coupling. In a resting cardiomyocyte, the sarcolemma membrane potential is around -80 to -90 mV due to the selective permeability of the membrane to K+ ions[8]. This resting potential is maintained by several factors, including the Na+/K+ ATPase pump and potassium leakage channels. When an action potential reaches the cardiomyocyte, it causes the membrane potential to rapidly depolarize due to opening of fast voltage-gated Na+ channels. This Na+ influx causes the membrane potential to overshoot to around +40 mV[20]. As the membrane begins repolarizing, slower activating L-type Ca2+ channels open, allowing influx of a small amount of Ca2+ into the dyadic space between the T-tubule and SR membrane. The exact trigger for SR Ca2+ release is still debated, but is thought to involve a conformational change in the L-type Ca2+ channel that mechanically activates the ryanodine receptor, and/or the small Ca2+ influx binding to and activating the ryanodine receptor. Activation of ryanodine receptors on the SR causes these Ca2+ release channels to open, resulting in a large efflux of Ca2+ from the SR into the cytosol. This amplification step, known as calcium-induced calcium release, produces around a 10-fold increase in cytosolic Ca2+ levels within milliseconds, providing the Ca2+ needed to initiate muscle contraction[12].

1.3.2 How action potentials propagate and lead to synchronized contractions across the heart

The heart's intrinsic conduction system precisely coordinates the sequences of electrical excitation and contraction to optimize cardiac pumping function. Rhythmic action potentials normally originate in the sinoatrial (SA) node, located in the right atrial wall, due to the automaticity of its. Specialized Excitatory and Conductive pacemaker cell[7]. The SA node exhibits the fastest intrinsic rate of self-excitation compared to other cardiac tissues, allowing it to drive the heart rhythm as the natural pacemaker. From the SA node, action potentials rapidly spread through internodal pathways, composed of ordinary atrial working cardiomyocytes but with increased conduction velocity, to reach the atrioventricular (AV) node located near the base of the right atrium. The AV node exhibits a small, compact structure with extensive cell-to-cell coupling, slowing conduction to create a necessary delay of ~0.1 sec that allows complete emptying of the atria before ventricular excitation[21]. After the delay in the AV node, action potentials rapidly propagate through the penetrating bundle of His and extensive Purkinje fiber network, large specialized fibers with high conduction velocities enabling synchronous activation of the ventricular muscle. This specialized ventricular conduction system allows the cardiac impulse to spread rapidly from the endocardial surface to the epicardial surface via the Purkinje fibers and ventricular muscle bundles in ~0.03 sec[22]. Consequently, all regions of both ventricles contract nearly simultaneously, generating efficient pumping pressure. The autonomic nervous system provides precise regulation of heart rate, conduction velocity, and contractility. Acetylcholine released from parasympathetic nerve endings hyperpolarizes membranes in nodal tissue and conduction fibers by increasing potassium permeability. This delays SA node self-excitation, slows AV conduction, and can even block impulse transmission if strong enough. In contrast, norepinephrine released from sympathetic nerve endings increases sodium and calcium permeability, acting on beta-1 adrenergic receptors. This accelerates SA node firing, speeds AV conduction by enhancing excitability, and increases the force of contraction. Abnormal pacemakers can occasionally take over rhythm generation if the SA node rate falters, causing inefficient excitation pattern. Heart block, where conduction fails at the AV node, can cause life-threatening deficits in ventricular pumping due to delayed activation. Thus the heart's specialized conduction system is essential for coordinated electrical and mechanical activity, with autonomic inputs providing rate control while intrinsic dysfunction disrupts optimal function.

1.3.3 Contraction in 2d monolayer

A 2D monolayer culture refers to plating human induced pluripotent stem cell-derived cardiomyocytes (hiPSC-CMs) on a flat surface, usually a cell culture dish or multi-well plate, to allow the cells to grow in a single layer[23]. This 2D setup provides a simple yet powerful in vitro model system to study cardiomyocyte structure, function, and drug responses outside of the body[24,25]. Human induced pluripotent stem cells (hiPSCs) are generated by reprogramming adult somatic cells such as skin or blood cells to an embryonic-like pluripotent state through the forced expression of specific genes. HiPSCs exhibit the ability to indefinitely self-renew and differentiate into all cell types of the body, similar to human embryonic stem cells[26]. To create a 2D monolayer of hiPSC-CMs, the pluripotent stem cells are first differentiated into cardiomyocytes using established cardiac differentiation protocols that recapitulate embryonic cardiac development. This produces a high yield of beating cardiomyocytes with typical cardiac marker expression from the hiPSCs. The purified hiPSC-CMs are then dissociated into a single cell suspension and plated on substrates coated with extracellular matrix proteins at an optimized density[27]. The cells adhere, spread, and proliferate to form an interconnected, synchronously beating sheet of human cardiomyocytes within days. Being cultured in vitro allows precise control of the microenvironment including chemical, physical, and electrical factors that influence cardiomyocyte growth, maturation, contractility, and electrophysiology. Thus, 2D monolayers present a simple, defined, and flexible platform for investigating human cardiomyocyte biology and screening drugs, mutations, and other factors for potential cardiotoxic effects[28]. There are a few key reasons why human induced pluripotent stem cell-derived cardiomyocytes (hiPSC-CMs) in 2D monolayer culture exhibit spontaneous beating:

- **Pacemaker cells** - During cardiac differentiation, a subset of hiPSC-CMs adopt a pacemaker-like phenotype. These cells express funny current channels like HCN4 that allow spontaneous depolarization during diastole to reach the threshold for an action potential.

- **Automaticity** - Single hiPSC-CMs display automaticity, meaning they can self-excite to generate their own electrical activity. This is likely due to expression of pacemaker currents that depolarize the membrane.

- **Cell-cell coupling** - Gap junctions electrically couple adjacent hiPSC-CMs, allowing depolarizing current to spread and trigger action potentials in neighboring cells. This allows a cluster of spontaneously activating cells to drive beating of the syncytium.

- **Immature phenotype** - hiPSC-CMs exhibit an immature, embryonic-like phenotype that may promote spontaneous activity. They have a less negative resting potential and underdeveloped inward rectifier K+ current that maintains pacemaking.

- **Electrophysiological instability** - Absence of external regulation from nerves/hormones combined with an immature phenotype renders hiPSC-CMs electrically unstable in vitro, prone to spontaneous activation. In summary, the presence of pacemaker-like cells, automaticity, cell-cell coupling, and an intrinsically unstable electrophysiology enables the emergence of spontaneous beating in hiPSC-CM monolayers. Maturation and electrical integration can reduce this spontaneous activity.

1.4 Challenges in Diseases and Toxicity related to Human Heart Contraction

1.4.1 Introduction to in-vitro models

The intricate nature of the human heart makes it susceptible to a wide array of diseases and toxic insults that can disrupt its vital functions. Cardiovascular diseases, including arrhythmias, heart failure, and cardiomyopathies, remain global health burdens with substantial impact on mortality and morbidity. At the same time, concerns about drug-induced cardiotoxicity have fueled a need for more comprehensive toxicity assessment methods. Addressing these challenges requires innovative approaches that leverage our understanding of cardiac physiology and the development of advanced in vitro models. Conventional approaches, including animal testing, have long been the norm in scientific exploration. However, these methods are fraught with limitations that hinder their ability to provide accurate insights into human cardiac responses. Among these limitations

are high costs, lengthy experimental timelines, ethical concerns, and the often inconsistent translation of findings from animal models to human clinical trials. A pivotal driver of this paradigm shift is the realization that traditional models often fall short in accurately predicting human responses to pharmaceutical interventions, ultimately impacting patient safety and therapeutic efficacy. Emerging as a transformative solution is the utilization of in vitro models, particularly human-induced pluripotent stem cell-derived cardiomyocytes (hiPSC-CMs). These models hold the promise of bridging the gap between conventional animal testing and the clinical reality. HiPSC-CMs are disease-specific and patient-specific cellular models that provide a closer representation of human cardiac responses. These models enable the investigation of disease mechanisms, drug responses, and toxicity assessments in a controlled and reproducible environment.

1.4.2 Disease Modeling and Mechanism Exploration

In vitro models play a pivotal role in simulating and dissecting the intricate mechanisms of various cardiac diseases, offering an invaluable tool to delve into the underlying molecular intricacies driving these complex conditions. Through the integration of patient-derived cells or the strategic introduction of targeted genetic modifications, these models provide an avenue for comprehensive exploration into how genetic mutations, intricate signaling cascades, and a myriad of contributing factors collectively shape a diverse spectrum of cardiac disorders. This approach facilitates a granular understanding of the intricate interplay between genetic factors, cellular pathways, and disease phenotypes, which can be crucial for unraveling the complex pathogenesis of cardiac diseases. For instance, the introduction of specific genetic mutations into in vitro cardiac models allows to observe and manipulate the resulting alterations in cellular behavior, ion channel function, and contractile properties, closely mimicking the conditions seen in various cardiac pathologies. By shedding light on the molecular and cellular dynamics underlying cardiac diseases, in vitro models offer a platform for advancing our comprehension of disease progression and the underlying mechanisms. These insights are pivotal for informing the development of targeted therapeutic strategies aimed at mitigating or even reversing the pathological changes observed in cardiac disorders. With the ability to recapitulate disease-specific conditions, in vitro models provide a controlled environment to test potential drug candidates, analyze their effects on cellular function, and ascertain their potential efficacy in ameliorating disease-associated abnormalities.

1.4.3 Facilitating Drug Development and Toxicity Screening

In vitro models have emerged as indispensable tools in the realm of drug development and toxicity screening for cardiac disorders[29]. Drug development refers to the complex and systematic process of discovering, designing, synthesizing, testing, and bringing new pharmaceutical compounds or therapeutic agents to market for the purpose of treating, preventing, or diagnosing various medical conditions and diseases. It involves a series of stages, from early research and preclinical testing to clinical trials, regulatory approvals, and post-market surveillance. The ultimate goal of drug development is to create safe, effective, and targeted medications that improve patient health and quality of life[30]. This process encompasses a wide range of scientific, medical, regulatory, and ethical considerations to ensure that new drugs meet rigorous standards for safety, efficacy, and quality before they can be made available for medical use[31]. Toxicity screening is the systematic process of evaluating the potential harmful effects of substances, such as drugs, chemicals, and other compounds, on living organisms, cells, tissues, or organs. Traditional drug testing methods, often reliant on animal models, are not only time-consuming but also fraught with discrepancies in predicting human responses due to species-specific variation[32,33]. One notable advantage of in vitro cardiac models is their capacity to facilitate high-throughput investigations of drug candidates[33,34]. Unlike conventional animal studies, which are often resource-intensive and slow, in vitro models permit rapid screening of a wide range of compounds, potentially expediting drug discovery processes. This is especially critical in the context of cardiac diseases, where the identification of effective therapeutics is paramount. In vitro cardiac platforms, such as microfluidic organ chips and engineered tissue constructs, enable to assess drug responses across a multitude of samples simultaneously. The integration of microscale technologies and automated systems further enhances the throughput of experiment[34,35]. This approach accelerates the evaluation of drug efficacy, safety, and potential adverse effects, thus reducing the time and resources required for preclinical drug testing[36]. In vitro models provide a more human-relevant environment for drug testing, thereby enhancing the predictive accuracy of drug responses. By utilizing patient-derived cells or genetically modified cell lines, one can replicate the genetic and physiological diversity observed in clinical populations. This is particularly relevant in studying cardiac diseases with a strong genetic component, such as inherited arrhythmias. Furthermore, in vitro models offer the flexibility to create disease-specific conditions that mirror the pathological state of cardiac disorders. By inducing disease-relevant cellular phenotypes, researchers can

simulate disease progression and assess the effects of potential drugs in a context closely resembling the clinical scenario. This tailored approach significantly improves the translatability of preclinical findings to clinical outcomes, bridging the gap between laboratory research and patient care.

1.4.4 Personalized Medicine and Patient-Centric Approaches

In vitro cardiac models have ushered in a new era of personalized medicine, revolutionizing the way we approach the diagnosis, treatment, and management of cardiac diseases[37]. The concept of tailoring medical interventions to individual patients, namely personalized medicine, has gained momentum, and in vitro models provide a powerful platform to implement patient-centric strategies. The advent of in vitro cardiac models enables the development of personalized diagnostic and treatment approaches based on an individual's genetic makeup and disease profile[26]. By using patient-derived cells, these models faithfully recapitulate the genetic predispositions and disease phenotypes of specific patients. This personalized approach allows clinicians to gain insights into the mechanisms underlying a patient's cardiac disorder and predict how the patient's cells will respond to different treatments[38]. In vitro models also facilitate the testing of a patient's sensitivity or resistance to specific drugs, ensuring that treatments are tailored to maximize efficacy while minimizing potential adverse effects. This approach empowers clinicians with the knowledge to select the most suitable therapeutic options for each patient, reducing the trial-and-error approach that can lead to suboptimal outcomes. The use of patient-derived cells in in vitro cardiac models has profound implications for drug development in the realm of personalized therapies. Traditional drug discovery often follows a one-size-fits-all approach, leading to drugs that may be effective for some patients but not for others. In vitro models allow researchers to test drug candidates on patient-specific cardiac cells, gaining insights into how individual variations impact drug responses. This approach holds significant promise for identifying novel drug targets that are specific to certain patient subgroups or genetic mutations. By simulating the interactions between drug compounds and patient-derived cardiac cells, researchers can prioritize drug candidates that demonstrate the greatest efficacy for a particular patient population, thereby fostering the development of more targeted and effective therapies.

2 Nanotechnologies for in vitro cardiac contractility

The contractile function of cardiomyocytes is of paramount importance, given their crucial role in circulatory physiology and the global prevalence of cardiovascular diseases. As the cellular units responsible for orchestrating each heartbeat, cardiomyocytes' contraction capacity offers invaluable insights into overall cardiac performance, both in healthy states and disease conditions. Since compromised contractile force production underpins numerous cardiac pathologies, there is a pressing need for enhanced tools to investigate the mechanics of contraction at the cellular level. The significance of assessing cardiomyocyte contractility has been underscored by several compelling factors. Foremost, drug-induced cardiomyopathy and cardiac toxicity represent substantial risks during pharmaceutical development, contributing to numerous failures of potential drug candidates in the past. Advancing the screening of the impact of small molecules and biological drugs on cardiomyocyte contraction mechanics could substantially improve the prediction of toxicity, thereby mitigating potential harmful effects. Additionally, the direct impairment of contraction in inherited and acquired cardiomyopathies highlights the urgency to delineate the molecular contributions to contractile function. Furthermore, the realms of tissue engineering and stem cell therapies for regenerative medicine necessitate the optimization of contractile properties in engineered or stem cell-derived cardiomyocytes to replicate normal physiological function. Lastly, fundamental questions persist regarding the translation of cellular contraction to the pumping of the entire organ, a challenge that nanoscale tools could help address by bridging the gap between molecular-level mechanisms and tissue-level responses. Microfabrication techniques and nanotechnologies emerge as pivotal tools to investigate the contractile properties of hPSC-CMs. Nanotechnologies enable the engineering of hPSC-CMs to create systems in which cellular properties and function harmonize with physiological characteristics. In essence, these techniques facilitate the development of innovative platforms that enable to delve deeper into the intricate mechanics of cardiomyocyte contraction.

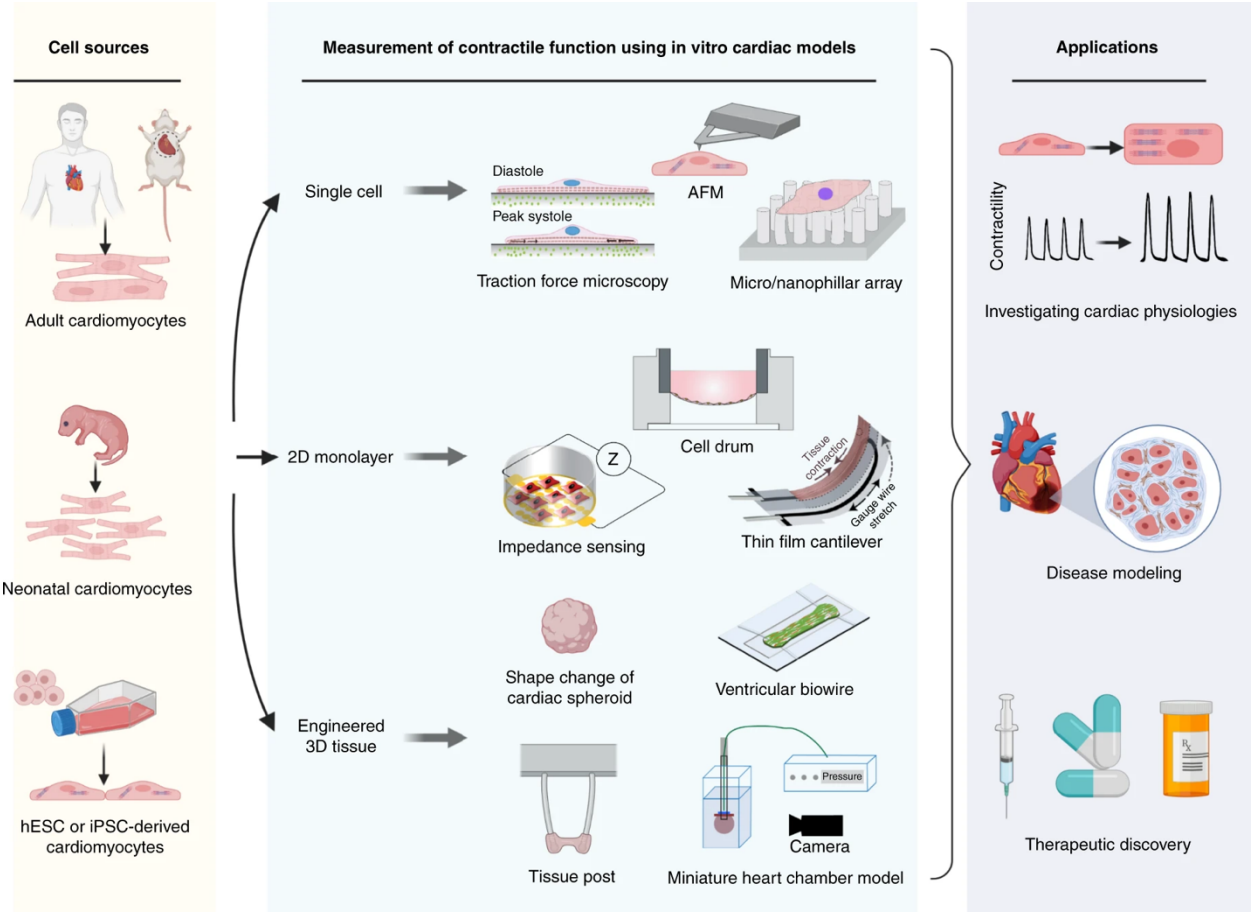

Figure 2.1 Cell sources of in vitro cardiac models include adult cardiomyocytes, neonatal animal cardiomyocytes and cardiomyocytes derived from human embryonic stem cells (hESCs) and from induced pluripotent stem cells (iPSCs). In vitro cardiac models are established in the forms of single cardiomyocytes, 2D cell monolayers and 3D cardiac models. The assessment of contractile functions of in vitro cardiac models can facilitate research applications for fundamental cardiac physiology studies, disease modeling and therapeutic discoveries. Reproduced with permission51,52,94,114. Copyright 2014 the American Physiological Society, Copyright 2017 Springer Nature, Copyright 2019 Elsevier, Copyright 2015 Royal Society of Chemistry. Figure created with BioRender.com.

2.1 Single cell

At the single cell level, specialized nanotechnologies are required to quantify the minute contractile forces and displacements generated by individual cardiomyocytes. Gold standard approaches include traction force microscopy (TFM), atomic force microscopy (AFM) and video based motion tracking[39,40].

TFM involves plating cells on flexible substrates coated with markers (i.e. distinct and identifiable points or objects strategically placed on a surface, or subject of interest). Contractile forces can be

computed by tracking substrate deformations caused by adhered cells[40]. However, the non-physiological stiff substrate and presence of markers may influence cell behavior[41]. By acquiring images of the substrate before and after force application, microscopic deformations caused by cell-generated traction stresses can be detected. Using the principles of elasticity theory, computational models, and knowledge of the substrate's mechanical properties, the markers displacements can be converted into cellular traction forces. Force reconstruction algorithms generate force vector maps indicating the magnitude and direction of forces exerted at adhesion points beneath the cell[42,43]. Thus, TFM provides high resolution spatiotemporal maps of cell-substrate traction stresses in the nano- to micro newton range. It has become a valuable tool for studying contractility and mechanotransduction in fields like cell motility, mechanobiology, and cardiomyocyte function. Using TFM, a relevant study demonstrated that increases myofibril alignment improves sarcomere activity and mechanical output[44]. Moreover, organizing hPSC-CM sarcomeres by engineering approaches improved not only contractile alignment and structure, but also calcium handling, mitochondrial organization, electrophysiology, and ultrastructure to levels closer to mature cardiomyocytes. The maturity enhancements extend beyond contractile proteins to multiple phenotypic hallmarks. Combining a nanopatterned substrate with a custom traction device J.M. Pioner managed to measure contractility and tension in single myofibril from hPSC-CM. In this study, Pioner et. al. conducted an investigation using hiPSC-CMs cultured on nanogrooved surfaces to explore their structural and functional maturation over an extended period[45]. Unlike earlier findings that indicated minimal T tubule formation in 2D-cultured hiPSC-CMs, the current study revealed a more complex architecture that could be linked to the development of transverse-axial tubular system (TATS), a crucial component for regulating ECC[45].

Another tool for studying single cell contraction is Atomic Force Microscopy. AFM has become a valuable technique for assessing the nanomechanical properties of cardiomyocytes with high precision, including measurements of elasticity, adhesion, plasticity, and viscoelasticity. AFM can quantify changes in cardiomyocyte stiffness between states of contraction and relaxation, demonstrate effects of cytoskeletal disruption, characterize responses to varied substrate stiffness, and elucidate alterations with cell age or due to disease mutations and drug exposure. AFM-based stress relaxation and creep experiments have further elucidated the viscoelastic characteristics of living cardiomyocytes[46].

One major application has been using AFM cantilever deflection to directly assess the beating profile of cardiomyocytes, enabling measurements of contractile force, frequency, kinetics, and cell displacement with high resolution[47]. Combining AFM with fluorescence imaging has allowed correlating contractile forces in beating cells with intracellular calcium fluxes. This approach has become very useful for assessing impacts of disease-causing mutations, drug toxicity, biomaterial substrates, coculture conditions, and other factors on cardiomyocyte beating dynamics. The capability to use AFM tips for localized stimulation of cardiomyocytes further expands the functional probing options. Recent advances in AFM imaging modes have also enabled visualization of cardiomyocyte morphological and mechanical properties at higher resolutions than previously possible[48]. Since 1999, AFM has been successfully used to study individual cardiomyocytes, showing that more variable pulsation frequencies, the shape features of pulses, like width and depolarization timing are consistent fingerprints of individual cardiomyocytes. Moreover, intrinsic differences in pulse shapes between cardiomyocytes persisted regardless of cell-cell contacts[49].

Finally, pure video based analysis is adopted to monitor myocyte contraction. Utilizing optical imaging to observe alterations in cardiomyocyte morphology or sarcomere dimensions during the cardiac contraction process has been employed as an indirect approach to assess cellular contractile performance[50]. Numerous kinetic metrics can be extracted from video recordings to characterize cell contraction, encompassing factors like the cell's shortening ratio, beating displacement, contractile strain, contraction velocity, beating frequency, peak-to-peak time, and sarcomere shortening. Post capturing a time-series of cardiomyocyte contractions through microscopy, image processing methodologies can be employed to quantify the dynamics of cell beating. These methods include analyzing periodic alterations in transmitted light intensity, utilizing edge detection algorithms to measure changes in cell shape, and employing digital image correlation to compute strain or displacement magnitude during contraction[51]. Quantification of fractional sarcomere shortening is also achievable through brightfield or fluorescence videos, allowing for the assessment of force generation. Video-based motion analysis serves as a noninvasive and label-free avenue for measuring contraction. This technique has been augmented by the development of sophisticated image processing algorithms and open-source software tools that streamline automated measurements[52]. Additionally, brightfield imaging can be coupled with other methodologies like patch clamps, MEA, and voltage/calcium-sensitive dyes to enable

simultaneous assessment of excitation-contraction coupling parameters. Even cardiac spheroids, characterized by well-defined boundaries facilitating image segmentation, have been subject to video-based motion analysis. Nevertheless, employing this approach to detect mechanical movements of cardiomyocytes within a monolayer configuration presents challenges due to the flat, thin geometry and high cell density. An inherent drawback of this method pertains to the uncertain correlation between kinetic parameters and contraction force[52]. Notably, variations in traction force and beating displacement from identical cell populations in response to stimuli like isoproterenol have been found to differ, underscoring potential measurement errors associated with estimating changes in contractility solely based on mechanical cellular movements[53].

2.2 Monolayer

A monolayer of cardiomyocytes refers to a two-dimensional (2D) culture arrangement in which cardiac muscle cells are grown as a contiguous, single layer on a substrate surface. In this configuration, the cardiomyocytes are closely packed and adhere to the substrate, allowing for interactions between adjacent cells and the establishment of intercellular junctions that are crucial for synchronized electrical signaling and coordinated contractile activity[25,54]. Conventional two-dimensional (2D) cardiac models have traditionally involved the cultivation of cardiomyocyte monolayers on standard culture dishes and multiwell plates. However, recent advancements in microfabrication techniques have revolutionized this approach by enabling the growth of 2D monolayers on micro-physiological systems, thereby affording precise regulation of in vitro microenvironments. These systems further facilitate the in situ measurement of cardiac functional attributes.

While 2D monolayer models possess certain limitations, such as their inability to provide 3D extracellular microenvironments[55] and support co-culturing of cardiomyocytes with other cell types, they do present an advantageous equilibrium between model complexity and the maintenance of crucial cell physiological functions essential for functional assessments. Consequently, they find frequent utilization in industries for the evaluation of therapeutic efficacy and cardiotoxic implications of potential drug candidates, leveraging the benefits of high throughput testing[56].

2.2.1 Electrical Impedence-based contractility

Electrochemical impedance spectroscopy (EIS) stands as a robust method employed in the assessment of interfacial characteristics associated with bio-recognition processes taking place at the electrode interface. These processes encompass events like antibody-antigen binding, interactions between substrates and enzymes, and even the capture of entire cells. Consequently, EIS holds considerable potential for diverse applications in the realms of biomedical diagnosis and environmental monitoring[57]. The utilization of interdigitated electrodes (IDEs) for electrical impedance measurement was initially conceived to assess alterations in cellular adhesion, morphology, proliferation, migration, and confluence. IDEs originally enabled the ongoing monitoring of morphological transformations in adherent cells, yielding quantitative insights from cultures with varying densities. This approach demonstrated the ability to detect minute vertical cell movements at an approximate scale of 1 nm[58]. In brief, following the application of a modest AC potential across the interdigitated electrodes (IDEs), an ion current is initiated between the pairs of electrodes. This ion current undergoes modifications upon the adhesion and expansion of cells on the electrode surface, a phenomenon that is quantified through the technique of electrical impedance spectroscopy[59]. Fluctuations in impedance magnitude arise from the dynamic beating of cardiomyocytes, resulting in alterations in their morphology. The cell index, which is determined as the relative change in impedance ($\Delta Z/Z0$) during the cardiac cell's beating cycle, is a widely utilized measure for quantifying the contractile activity of the heart[60]. Impedance based biosensors have been successfully adopted for compounds screening in toxicity assessment of cardiomyocyes [61].

2.2.2 Flexible Thin-film based sensor

The culture of cells on substrates of very high rigidity is suspected to significantly change mechanical characteristics. The same restriction applies to atomic force measurements (AFM) of cellular monolayers, where the stiff substrate is a fundamental prerequisite for accurate force transduction. Thin-film biosensors for cardiomyocytes contractility encompass a wide range of platforms that employ various readout mechanisms. While these platforms share the common feature of utilizing a thin polymeric film for cell cultivation, the readout mechanism for membrane displacement varies among them. Indeed, the contraction of a 2D monolayer can be characterized

by the mechanical deflections of a flexible thin film induced by cell beating. The most common technique to measure a membrane displacement involve:

- Pressure based sensors[62]
- Laser deflection sensors[63]
- Piezoelectric strain sensors[64]
- 2D cantilevers with optical based read out

CellDrum technology is an example of pressure and laser based sensor[62]. It provides cells a precisely defined biomechanical environment, while maintaining a high level of experimental simplicity. Cells are cultured on a well-defined reference material, composed of an ultra-thin silicone membrane that seals the base of a cell culture well. As cardiomyocytes rhythmically contract, they cause the membrane to elevate due to the weight of the culture medium. This deflection is continuously tracked using a laser triangulation sensor, while the pressure beneath the membrane is also recorded. By applying Laplace's law to the recorded data, the membrane tension can be calculated[62]. Another study shows a novel dual-function biosensing platform, designed to concurrently monitor both contraction force and field potential signals of layered CMs. To emulate the natural heart environment, the diaphragm structure is crafted from PDMS, patterned of 800 nm nanogrooves. The displacement of the PDMS diaphragm resulting from CM contraction force is precisely detected using a highly sensitive laser vibrometer [65]. Others introduced a system capable of assessing the contractile force and extracellular field potential of dynamic beating cardiac cell sheet-tissues. To achieve this, cardiomyocytes were cultured on a 500 nm-thick parylene film. The rhythmic beating of the tissue was verified, with sufficient intensity to reliably quantify the contractile force. This system simultaneously captures extracellular field potential and contractile force. Contractile force measurements was achieved connecting the 500 nm-thick parylene film to a load cell [66].

To measure cardiomyocyte contraction from electrical readouts, flexible strain sensors have been integrated into both thin membranes and the cantilever platforms. Dou et. al. introduced a novel flexible bioelectronic platform in a 24-well plate format[43]. This platform enables continuous and

high-throughput measurements of contractile function. The authors developed of flexible strain sensors, leveraging a piezoresistive sensitivity of zero-dimensional carbon black (CB) particles. The exceptional conductivity and electrochemical stability of carbon fibers were harnessed to create stimulating electrodes. The core of the platform comprises ultrathin and suspended membranes, integrated with flexible CB-polydimethylsiloxane (PDMS) strain sensors, facilitating both cell culture and in situ assessment of cardiomyocyte contractility. Pneumatic pressure channels and carbon fiber electrodes were seamlessly integrated to provide precisely defined mechanical and electrical cues, effectively regulating iPSC-CM physiology and enhancing their maturation[53,67].

Another strategy that has been widely adopted to measure cardiomiocytes contractility is based on flexible cantilevers. In micro engineering, a cantilever refers to a slender and rigid structure that is anchored at one end and free to move at the other end[68]. It is a common component used in various microfabrication and nanotechnology applications, particularly in micro-electromechanical systems (MEMS) and nanoelectromechanical systems (NEMS)[63]. In these platforms, cardiomyocytes (CMs) are cultured on a polymeric cantilever, which is commonly functionalized to enhance cellular adhesion. During contraction, CMs cause the cantilever to bend, resulting in a specific amount of displacement. This displacement is typically quantified at a specific sensor point using a laser vibrometer[65]. Different shapes of SU8 polymeric based cantilever have been proposed and successfully measured the CMs contractility. Utilizing μgroove patterns aids in aligning cardiomyocytes atop the SU-8 cantilever, resulting in an approximately 2.5-fold increase in their contraction force. The SU-8 cantilevers are also employed to investigate the impact of different drugs on cardiomyocyte contraction force. The findings demonstrate the effectiveness of this approach for real-time screening of drug toxicity in cardiomyocytes [69,70]. Regarding the sensing mechanisms, alternate techniques like optical imaging or the incorporation of embedded strain sensors can be employed to detect the bending. The accurate evaluation of cardiomyocyte contractility on the cantilever surface can be achieved through precise optical tracking of the bending magnitudes. However, it's worth noting that utilizing a microscope or laser source necessitates repetitive and time-consuming alignment procedures. When considering the use of embedded strain sensors, the approach involves depositing gold thin-film strain sensors onto PDMS cantilevers and isolating them with a thin PDMS layer.

2.3 3D culture – organ on a chip

The advancement of microfabrication technologies and tissue engineering has paved the way for engineered 3D cardiac tissue models [25]. These models are developed through different methods such as encapsulating cells within hydrogels, culturing cells on decellularized matrices or artificial scaffolds, and utilizing the self-assembly properties of cells to form scaffold-free tissue aggregates[54,71]. Compared to traditional 2D monolayers, 3D cardiac tissues better replicate the physiological microenvironment, native tissue organization, and tissue functions. The incorporation of various cell types has also been explored to enhance tissue properties[72].

Engineered heart tissues (EHTs) are created by encapsulating cells such as cardiomyocytes, cardiac fibroblasts, and endothelial cells in collagen/fibrin hydrogels tethered to anchoring constructs [73]. EHTs have been developed for tissue physiology analysis, drug screening, disease modeling, and cardiac repair. Various heart-on-a-chip platforms have been developed to integrate on-chip force-/stress-sensing components for in situ measurement of EHT contraction dynamics [74]. One well-known model is the cardiac tissue suspended between two flexible posts/cantilevers, where cardiomyocytes are mixed with fibrin and collagen hydrogels and pipetted into casting molds in which a pair of flexible silicone posts or T-shaped vertical cantilevers are positioned[54]. After tissue compaction, cardiac muscle strips are wrapped around the silicone posts/cantilevers, exhibiting better longitudinal alignment induced by passive mechanical tension. The deflection of the silicone posts or upright silicone cantilevers induced by the cyclic contraction of EHTs is video-recorded, and the post/cantilever mechanical properties, bending magnitudes, and bending frequencies are used for calculation of the contractile force and beating rate of the EHT. To improve throughput for drug testing, elastic post/cantilever platforms have been developed to construct arrays of EHTs in standard 24-well or 96-well plates. Custom-made software has also been developed to enable image acquisition and evaluation of contractile force with increased throughput. Other modifications have been proposed to improve platform functionalities for tissue contraction measurement, such as the use of light-based 3D printing technology to fabricate a microscale force gauge made of one thin pillar as a bendable cantilever and one thick pillar as a fixed anchor. Another representative heart-on-a-chip model is the flexible wire platform, such as the Biowire II platform, which consists of an array of microwells patterned on a polystyrene sheet

by hot embossing and two flexible polymer wires located at each end of the microwell. Cylindrical trabecular tissue is formed in each microwell and suspended between two parallel polymer wires. Tissue contraction measurements are performed by converting wire deformation into force, and the polymer wires maintain an unaltered Young's modulus and force-displacement relationship for accurate force measurement during long-term tissue culture.

Finally, the self-assembly property of cardiomyocytes cocultured with stromal cells or fibroblasts is used to form scaffold-free 3D cardiac spheroids using the hanging drop method or nonadhesive micromolds/substrates. The spheroids have diameters ranging from 200 to 400 μm, within the hypoxic limits of tissue spheroids. Incorporating endothelial cells helps form microvascular networks inside the cardiac spheroids and increases the permeability of oxygen and nutrients into the core region. The tissue dimensions of the cardiac spheroids ensure high imaging contrast under brightfield or phase contrast microscopy for measurement of beating kinetics. Time-series images of the spheroid shape changes induced by tissue contraction are recorded, and edge detection algorithms are applied to detect the dynamic changes in spheroid boundaries during spontaneous contraction or contraction under electrical stimulation. The tissue contraction magnitude is calculated as the fractional area change of cardiac spheroids between the systolic and diastolic states. However, visible shape changes of spheroids do not directly correlate to tissue contraction force or stress, and other factors such as cell density, tissue composition, and culture time can influence the magnitude of size changes during spheroid contraction[51].

3 Interferometric biosensor for Cardiac Contractility

3.1 Significance

Heart disease, also known as cardiovascular disease (CVD), is a group of conditions that affect the heart and blood vessels. It is one of the leading causes of death worldwide. According to the World Health Organization, an estimated 17.9 million people die every year from CVD, accounting for 31% of all global deaths[75]. Those who study CVD and develop treatments need a relevant model of the cardiac muscle and the suitable technology to investigate its physiological and pathological conditions[76].

Over the past decades, hiPSC-CMs have been widely acknowledged as the best candidate to model the fundamental properties of the cardiac muscle[26], in contrast to animal models that present differences specific to their species[37]. Resembling some features of the human heart, hiPSC-CMs maintain the ability to contract spontaneously, thanks to a complex interplay between various proteins and ions[10]. The effectiveness of the contraction is pivotal to establish the well-being of the CMs tissue and it is evaluated measuring the following parameters: contractile force, dynamic of contraction, beating rate, passive tension, synchronicity, and beating propagation. Detecting alterations in any of these parameters can discriminate potential indications of disease or toxicity risk during a drug assessment[77]. While hiPSC-CMs provide a unique opportunity for disease modeling with isogenic cells, they still demonstrate distinct properties that make them functionally less akin to adult cardiomyocytes. However, numerous innovations in differentiation and modification of hiPSC-CMs and culture techniques have been developed to address this challenge[78]. These cells have been used to model inherited heart diseases and have the potential to revolutionize cardiovascular drug discovery, enabling the investigation of patient-specific conditions in a lab environment[79,80].

During the past decade, many *in-vitro* platforms have been developed with the aim of monitoring and quantifying the contraction force of hiPSC-CMs monolayer[41,43,53,66,67,81,82]. Regarding force measurements on CMs monolayers, the main approaches are electrical impedance-based sensors[67,83], image-tracking based sensors[84] and thin-film based sensors. Moreover, although they

present some limitation[60,85], gold standards for CMs contractility are atomic force microscopy (AFM) and traction force microscopy (TFM)[40,85]. Such distinction does not preclude that, in several devices, these approaches have been combined, toward the design of a low invasive, high throughput, and user-friendly heart-on-a-chip platform[71]. Nevertheless, all previously reported CMs sensors have some drawbacks. Whereas multiwell impedance sensors assess effectively drug effects and cardiotoxicity[42], interpreting impedance data can be difficult because electrode size, sweeping frequency, and cell density can influence signal patterns[53]. Image-tracking based sensors overcome such limitations since the read-out method is purely optical but many of these devices require the insertion of markers[40] (as fluorescent molecules) in the cell environment, while others employ PDMS patterned 3D pillars that do not mimic the physiological condition of CMs monolayers[39,82]. Pure optical based software has been developed to infer CMs monolayer contractility, but the relationship between kinetic parameters and contraction force remains difficult to quantify [83].

The thin film based sensors stand out as the most promising technique for contractility assessment in terms of invasiveness, throughput, and easy manufacturing. In such sensors, CMs monolayer is cultured on a thin polymeric membrane[41,81]. The CMs beating induces a membrane displacement which is measured by capacitive-, resistive- or optical-based technique and converted into a force by direct or indirect calculation. For instance, Zhao *et. al.* [65] employed a laser vibrometer to measure the displacement of PDMS thin film. Other PDMS based optical sensors have been studied and demonstrated the possibility to monitor the contraction of CMs; however, the precise relationship between the thin film displacement and contraction was not established[86]. Optical thin film-based biosensors remain the most promising approach to achieve label-free, high throughput, and accurate measures of the contractility of CMs.

In this section, a new device concept is presented. The device is based on arrays of optical interferometers that enable label-free high-resolution imaging of spontaneous and paced hiPSC cardiomyocytes contraction in vitro. The device, schematically depicted in Figure 3.1, is an array of *micro-interferometers* placed underneath the cell culture. Each interferometer is composed of two reflecting surfaces (gold squared mirrors) parallel to the cell culture plane and a fluorescent solution fills the space in between. The upper surface is free to oscillate while the bottom one is fixed. The mechanical property of the oscillating surface is engineered to respond to the cell

contraction. The cell beating modifies the position of the oscillating surface and, consequently, modulating the intensity of fluorescent light resonating into the interferometer. In other words, the cell beating imposes a rhythmic vibration to the optical cavity. By monitoring the cavity modulations one can monitor the cell beating. Notably, the proposed architecture converts the longitudinal forces, arising during the cell beating, into a vertical displacement of the upper surface, enabling the determination of the traction stress over the actual direction of the monolayer contraction. The array of resonators can be monitored by using monochromatic light and CMOS cameras so to achieve high resolution imaging both in space and time (3200 x 3200, 6.5µm x 6.5µm pixel; 498fps in the experiments presented in this thesis). Finally, no direct interaction occurs between the cells and the sensing system so the approach has very low invasiveness.

In my thesis I present the development of the device and a set of experimental data and numerical calculations on on mechanical and its optical behavior in the presence of beating cardiomyocytes. The results show that numerical calculations agree with the experiments. Importantly, by taking profit of both experiments and simulations, a comprehensive understanding was gained about how the contractile forces exerted by the cardiomyocytes are transduced into measurable changes in the optical interferences. The measured contractility traction measured by the vertical membrane displacement was in the range of 34 ± 4 mN/mm^2. This traction stress value is compatible with other measurements performed on similar cardiac cellular models using well-established techniques (https://innovitro.de/wp-content/uploads/2021/10/210911-innoVitro-Contractile-Force-Flyer.pdf).

3.2 Device Concept

The device technology, described in Figure 3.1, is based on the concept of "optical cavity" in classic Optics: an optical cavity is an arrangement of mirrors or other optical elements that form a cavity resonator for light waves. Inside the resonator, interference phenomenon occurs, creating a patter that can be modified consistently with the parameter of the optical cavity (e.g. the distance between the two mirrors)[87,88]. Following this idea, a device made of two optical interfaces was designed. Cardiac cells are cultured on the upper and flexible interface that is made of a thin silicon nitride membrane patterned with squared gold mirrors on both sides. At the interface with cells, squared pads of highly rough porous gold enhance the cells adhesion to the membrane. The upper

interface also delimitates and enclose the cell environment, namely the trans-chamber. The second and fixed interface, placed below the cavity, is a square glass substrate coated with a thin layer of gold. The cavity, namely the cis-chamber, defining space between the two interfaces, is filled with a fluorescent molecule (rhodamine, R6G, 0.2 mg/ml) dissolved in a non-volatile liquid (ethylene-glycol). As shown in Figure 3.1a, when irradiated by the correct wavelength light enhancing fluorescence emission of R6G (λ_{ex} = 543/22 nm), an interference pattern is created between the two interfaces. The fluorescence signal belonging to the volume under each gold mirror is reflected to the camera detector. Thus, a spatial down-sampling of the pattern is performed, as shown in Figure 3.1b. While the cardiac cells are resting, the interference pattern, and thus the optical signal, is steady. During the contraction phase, shown in Figure 3.1c, cardiac cells apply longitudinal forces to the silicon nitride membrane that leads to a local change of the distance between the two faces of the optical cavity. Hence, during the cell contraction, each gold mirror behaves as the oscillating part of an interferometer, in which the distance *l* changes (inset Figure 3.1a). As a result, the optical signal derived from each *micro-interferometer* changes according to the cells contraction. When the cells contraction ends, the silicon nitride membrane returns to its original configuration and, consequently, the signals are restored to the reference value. In this perspective, the device allows monitoring an entire cell culture contraction by using a matrix of *micro-interferometers* which changes its parameters according to the cells activity.

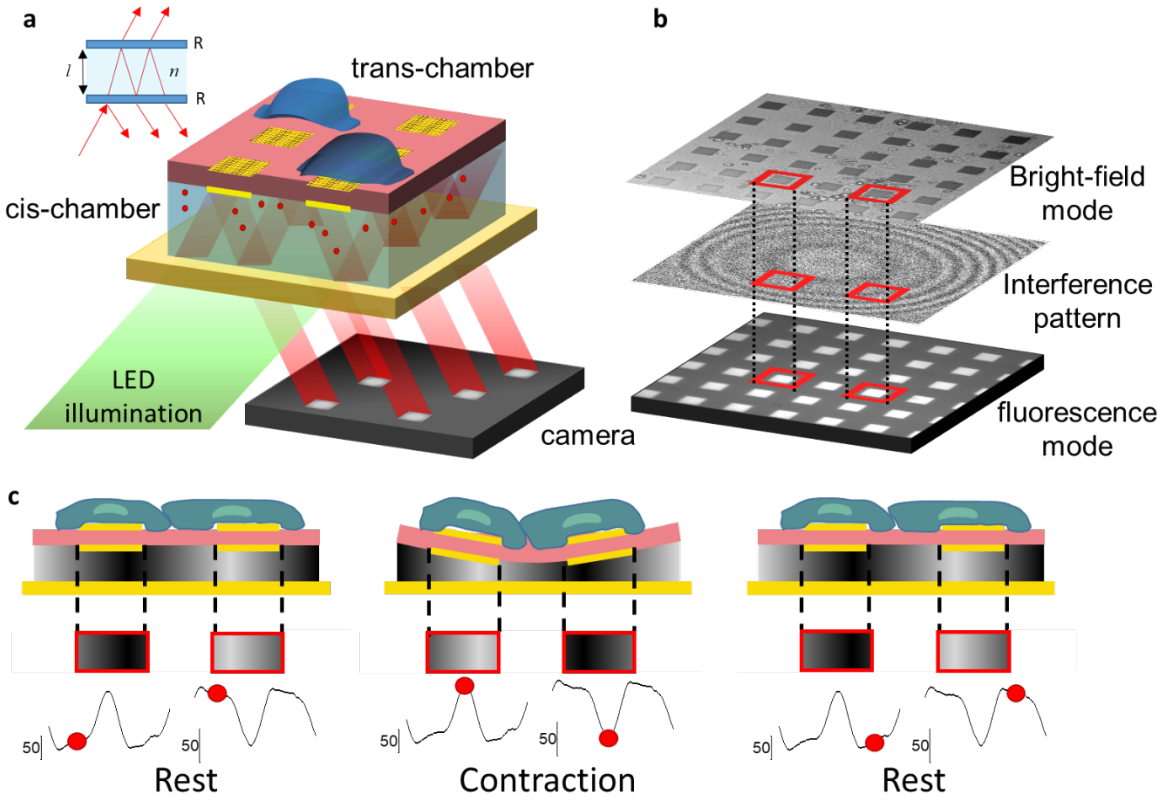

Figure 3.1 Device working principle. (A) 3D scheme of the device representing the silicon nitride membrane (red) with the embedded matrix of gold mirrors. On top of it, in the trans-chamber, the cell environment contains a 2D monolayer of hiPSC-CMs (shown only two exemplary cells). The cell monolayer is attached to the silicon nitride membrane and to the porous gold squared pads. The cis-chamber under the membrane is filled with ethylene glycol where we dissolved 0.2 mg/ml rhodamine (red dots). When the chamber is irradiated by the tailored light beam, the fluorescence in the cis-chamber is enhanced. The array of square gold mirrors reflect the fluorescence signal that is acquired by a CMOS camera. (B) Schematic overview of the signal acquired by the camera: first, in bright field mode it is possible to image the cell culture, second the interference pattern created in the cis-chamber, third the down sampled interference pattern reflected to the camera sensors. (C) Phase shift of the optical pattern and the relative fluorescent signal reflected by two single gold pads during the contraction event. During the contraction, the cells exert a force that bends the membrane, obtaining a variation of the cavity size. The variation of the cavity determines a change in the light intensity acquired by the camera (scale bar: photo-counts).

3.3 Device Fabrication

3.3.1 Membrane and interferometers fabrication

The silicon nitride membrane, 500nm thick, was fabricated from a double-sided silicon nitride-coated wafer, as previously described[33,89]. Each single membrane has an area of 2x2 mm² and is placed in a silicon contour of 2x2 cm² (Figure 3.2b). Then, after coating the membrane with 5 nm of titanium and 20 nm of gold, deposited by e-beam evaporation (Kurt J. Lesker PVD 75), the

sample underwent electrochemical gold deposition (Figure 3.2 a2). The deposition was performed using a plating bath containing K[Au(CN)2] dissolved in water (Parador HS – [Au] = 3 g L−1, pH = 4.2). The sample was connected to a current generator alongside a counter electrode, with the sample at the negative terminal and the counter electrode at the positive terminal. The electrodeposition process was carried out by setting the current to 35 mA for a duration of 6 minutes. Throughout the process, the plating solution was maintained at a temperature of 38°C and stirred at a moderate speed.

Subsequently, two consecutive lithography processes were carried out (Figure 3.2 a3-6). Firstly, a primer solution (H.M.D.S. TECHNIC) and an image-reversal photoresist (MicroChemicals AZ5214) were spun at 4000rpm for 1 minute and baked at 112 °C for 1 minute. A mask was designed with a matrix of empty square-shaped structures of 30µm in size, and exposure was performed. Afterward, the photoresist was inverted through a post-exposure bake at 120 °C for 2 minutes, followed by a flood UV light exposure of 30 seconds. After developing in AZ5214 Developer (MicroChemicals) for 45 seconds, gold etching for 30 seconds (Merck, gold etchant standard) was performed.

3.3.2 Mirror lithography

Once the first pattern was completed, it was used as a mask for the second lithography on the hollow part of the membrane. This side of the device is not suitable for standard lithography since it is not flat. Therefore, Lor3B was spun (1 minute, 3000rpm) and baked (3 minutes, 180 °C) on the hollow side of the device. Subsequently, an image-reversal photoresist (MicroChemicals AZ5214) was spun at 4000 rpm for 60 seconds and then baked at 112 °C for 1 minute. The sample was exposed without a mask under UV light for 10 seconds with the flat side upward. This process mirrored the pattern from one side of the membrane to the other (Figure 3.2 a5). After following the photoresist protocol, it was inverted and developed as described above. Then, the sample was coated with 5nm Ti and 20nm Au by e-beam evaporation from the hollow side. Afterwards, 50nm of Ag/Au alloy was sputtered onto it. The surplus material was then removed by lift-off in MF319 (Figure 3.2 a6). The silver was de-alloyed by immersing the sample in a 1:1 solution of HNO3 for 30 minutes. Finally, the sample was coated with a 3nm layer of SiO2 by ALD (Atomic Layer Deposition). The well for cell culturing was created by attaching a glass ring with a 10mm diameter

using a not-cured poly(dimethylsiloxane) (PDMS) preparation (Sylgard 184) baked at 70˚C for 2 hours (Figure 3.2b).

The bottom mirror was created from a squared 2 cm side substrate made of SiO2 coated with 100nm of ITO by RF Argon sputtering. Finally, a layer of 5nm Ti plus 20nm Au was deposited on the ITO film by e-beam evaporation. Then, 3nm of SiO2 was deposited by ALD. Before measuring, the bottom mirror was treated with oxygen plasma (time = 300 seconds, power = 100 W, O2 gas pressure = 100%) to enhance the surface wettability.

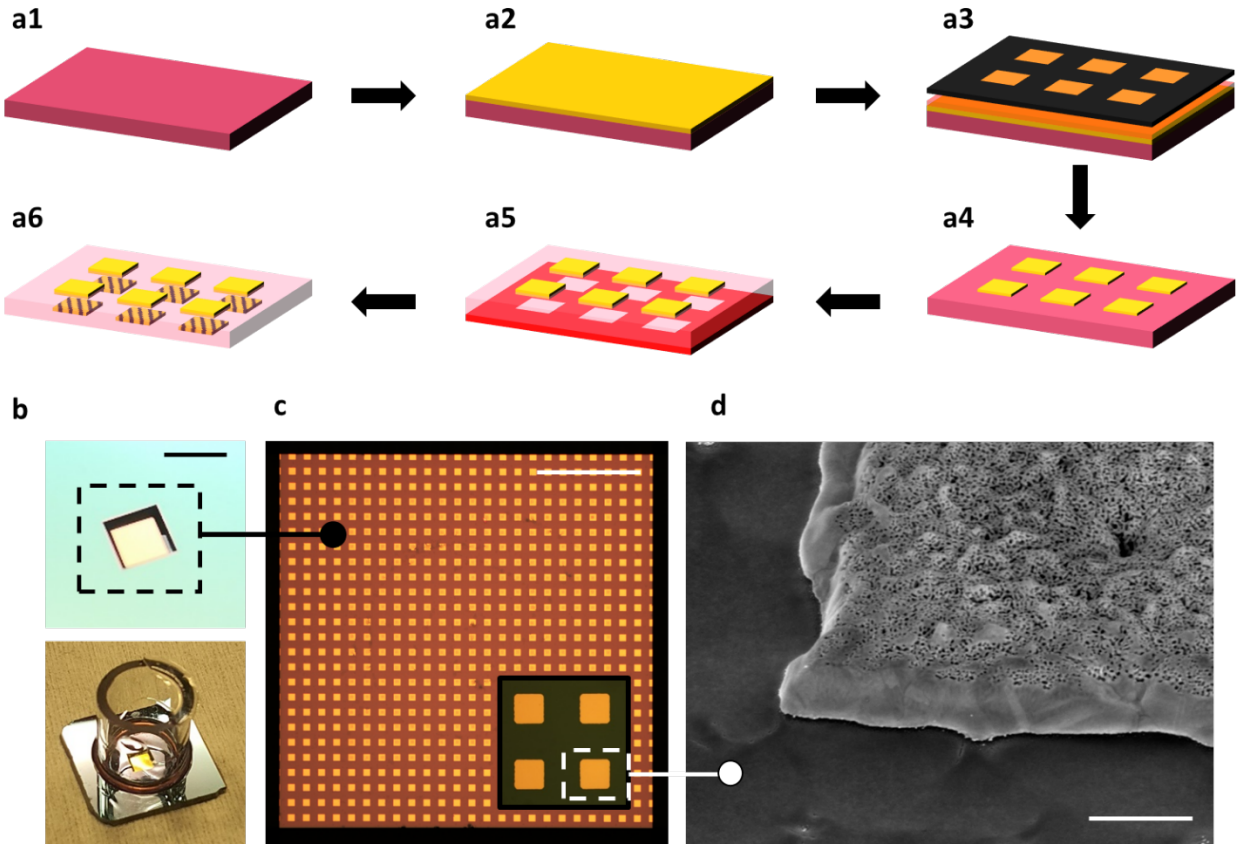

Figure 3.2 Device fabrication: (a) lithography process that allows to transfer the top pattern to the bottom side of the membrane. (a2) The silicon nitride membrane is covered with a thin layer of gold; (a3-a4) Optical lithography, followed by a wet etching process, allow to obtain a matrix of squared gold mirror; (a5) the sample is coated with photoresist on the bottom side, and the matrix of gold squares is used as mask for the photoresist; (a6) After developing, deposition of adhesion layer followed by the a silver-gold alloy is deposited on the bottom side. The mirrored pattern is obtained by lift-off process. Thereafter, the silver is de-alloyed in a nitric acid solution, leading to a porous gold surface. (b) Image of the device from the trans-chamber and detail of the silicon nitride membrane (scale bar: 2.5mm). (c) 5x optical microscope image of the gold pattern micro sensor (scale bar: 400μm). (d) SEM image of the porous gold layer deposited on each gold pads (scale bar: 100nm).

3.4 Contractility assessment

3.4.1 Spontaneous recording of contraction

To demonstrate the capability of the device, hiPSC-CMs were employed. The biocompatibility of the substrate had been previously assessed in a distinct study, substantiating cell viability at approximately 90% after 7 days in vitro (DIVs). Following 13 DIVs, the assembly of the sample with mature cells onto the microscope stage for measurements was conducted. A small quantity of fluorescent solution (0.2 mg/ml, R6G in ethylene-glycol) was introduced onto the bottom mirror, and the silicon nitride membrane containing the cells was positioned above, encapsulating the liquid between the two surfaces. Initially, the sample was illuminated from the top in transmission configuration to observe the cells on the membrane. Subsequently, during the measurement, bottom illumination with a wavelength of $\lambda ex = 543/22$ nm was applied to amplify fluorescence emission from R6G molecules and generate the interference pattern in the optical cavity (Figure 3.3). Upon bottom irradiation, acquisition of each micro-interferometer signal in the camera's field of view occurred simultaneously at a frame rate ranging between 50 and 1000 fps. The duration of each recording spanned from 30 seconds to 120 seconds, contributing to a total experimental time of up to 30 minutes. Figure 3.3a depicts the fluorescent signal intensity emanating from a singular micro-interferometer.

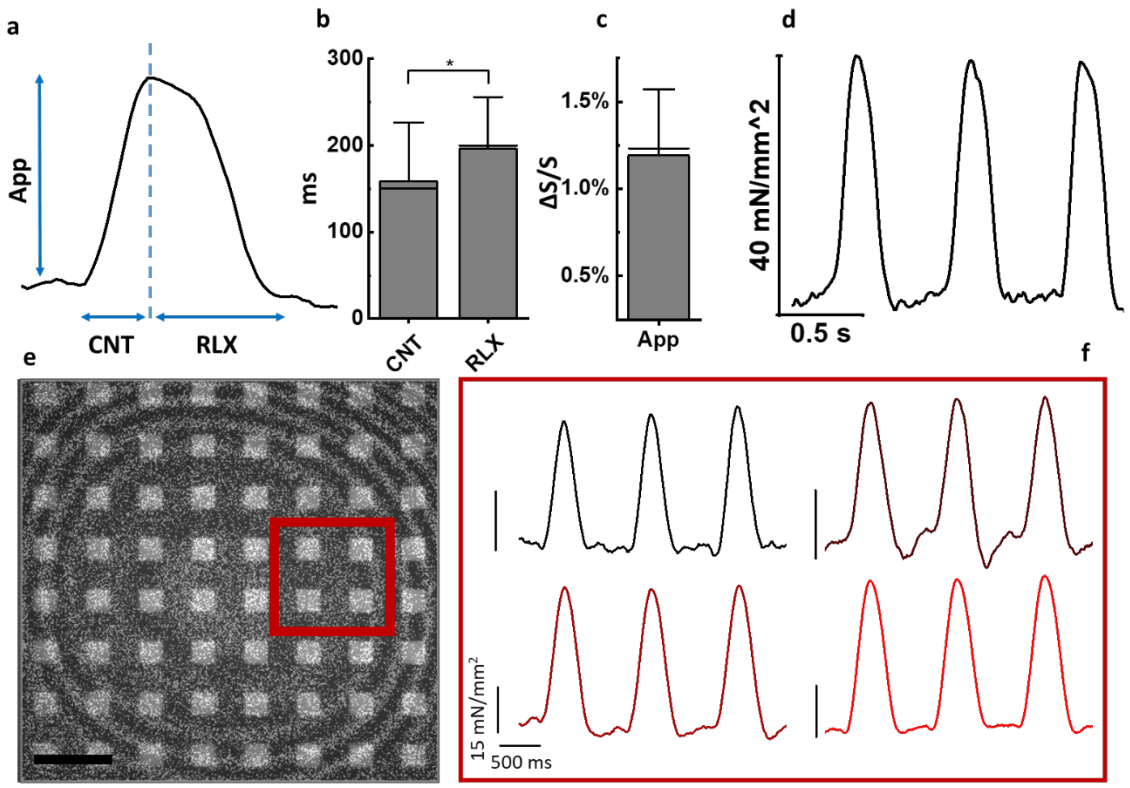

Figure 3.3 Recording of contraction activity of hiPSC-CMs (FUJIFILM Cellular Dynamics, Inc. (FCDI)) (a) Trace of a single contraction event. (b) Bar plot that quantifies the difference between contraction time (CNT) and relaxation time (RLX) (Kruskal-Wallis, $p<0.01$). (c) Bar plot to quantify the signal to noise ratio of the fluorescence signal defined as ΔS/S. (d) Example trace of 3 contraction events from a single micro-interferometer. (e) Fluorescence image of the device with superimposed the interference pattern (scale bar: 90µm). (f) Four contractility traces from the same recording showing the variability of the signal across an area of the device (x scale bar: 0.5 s; y scale bar: 15mN/mm^2).

During cell contraction, changes in the fringes of the interference pattern (Figure 3.3) are induced by membrane oscillations, resulting in variations of fluorescence intensity in each individual pad. The periodic beating of cells is monitored by observing the periodic variation of fluorescence intensity. It is noteworthy that the vertical displacement of the membrane (l) is smaller than the size of half the wavelength, causing fluorescence to oscillate with only one peak during each instance of cell contraction. In other words, the fluorescence blinking and cell beating occur in phase.

The variation of the spatial phase of the interference pattern is measured by monitoring the movement of the fringes, i.e., the signal of a micro-interferometer. If the size of the interference bands is approximately equal to the size of each micro-interferometer (30µm), the horizontal

movement of the bands causes the micro-interferometers to transition from a dark to a bright band or vice versa, thereby maximizing sensitivity (see section 3.4.2). Indeed, if the displacement (l) is small enough, the change in phase does not exceed one period of the local wave, resulting in a fluorescent signal with only one peak during each instance of cell contraction.

Fluorescence intensity fluctuations synchronized with cell contraction are measured, as observed through bright field imaging. Consequently, the signal frequency is contingent upon the spontaneous beating rate of the cell culture, which was approximately 1 Hz at 37°C in our experiments. Details of a single contraction event, showcasing the device's capability to distinguish between contraction and relaxation, are illustrated in Figure 3.3a. The signal-to-noise ratio (SNR), computed as the ratio between the fluorescence peak-to-peak signal of a contraction event (App) and the noise intensity during cell rest, is approximately 10. Furthermore, as extensively detailed in section 4.4, the mechanical properties of the membrane and the optical characteristics of the cis-chamber enable the quantification of the contractility strength of the cardiac cells. Three contraction events recorded from a single gold sensor at 13DIVs reveal a peak contractility of 38mN/mm2 in Figure 3.3d. Throughout the entire device, the amplitude and shape of the contractility signal may slightly vary based on the location of the individual sensor. In Figure 3.3e, four traces are presented, demonstrating matched interference patterns and interferometer sizes, yielding a contractility of 34±4 mN/mm2.

3.4.2 Identifying the area of maximum sensitivity

In his paragraph I will illustrate how the sensitivity changes across the device and how the maximum sensitivity area was identified.

Among the optical read-out methods, our approach stands out as the first interferometric based biosensor designed to measure and quantify the forces applied during the contraction of a 2D monolayer cardio myocyte culture. Briefly, interferometric biosensors measure small variations occurring in an optical beam during his pathway. When the optical path of a light wave λ is confined between two interfaces separated by a distance l, in a media with refractive index n, his phase φ can change following Equation 1:

$$\varphi = \frac{2\pi l n}{\lambda}$$

Although changes in the refractive index are commonly used to detect variations in the phase, small changes in the distance *l* between the two mirrors can drive the cavity off resonance and phase-shift light out of the interferometer, leading to considerable alterations in the beam characteristic 6. In our device, the distance l, the distance between the two interfaces, can change under the longitudinal forces applied by CMs contraction. The intrinsic properties of the micro-interferometer sensor allow the device to have a suitable dynamic range at the nm scale.

In this study, we fabricated and successfully measured 9 devices. Although we managed to create the interference pattern across the different devices, its precise location and shape slightly changed. Such minor variations can be attributed to several reasons. Firstly, the devices were fabricated from commercial wafers (Silicon Materials), which exhibit a variability of ±25nm in the thickness of the silicon nitride layer. Secondly, the membrane itself can bend in different modes when in contact with a fluid (ethylene glycol). Lastly, the local forces of cardiomyocytes and their distribution across the membrane differ in various cultures, even though the plating parameters remain consistent. While the aforementioned phenomena are beyond our control, the strategy of patterning the entire device surface and creating a matrix of micro-interferometers ensures that the device can detect the signal wherever the interference pattern is effectively generated. During measurements, we recorded different areas across the device separately, using acquisition sets lasting 1-2 minutes each, resulting in a total recording time of approximately 30 minutes. In the post-processing of the data, we identified the areas of maximum sensitivity of the device, as explained in Figure 3.4. These areas of maximum sensitivity align with the size of the interference pattern, and the identification process was carried out as follows: First, we employed ImageJ software for background subtraction, subsequently, we used the Tox-Free software to automatically identify the region of interest and extract the relative fluorescence intensity traces. The final measure of contractility is averaged across the micro-interferometers displaying maximum sensitivity. In Figure 3.5, we provide an example of the post-processing steps required to identify the areas of the device from which to extract the contractility signal. Initially, we opened the video in ImageJ and subtracted the first frame from the video to eliminate the absolute value of the light intensity across the images (Figure 3.5a). In this configuration, the interference phenomenon became clear, and we identified the pads with the potential for higher sensitivity (Figure 3.5b, marked with green squares). We selected the same pads in the custom Tox-Free software, where we extracted the fluorescence traces (Figure 3.5c). This example (Figure 3.5c)

shows the signal derived from the four selected pads with a clear signal-to-noise ratio (S/N). Averaging the signal from these four pads provided a more precise measure of the contraction activity. A supervised machine-learning algorithm such as the implementation of a neural-network would be useful to discriminate different sensitivity areas: neural networks can take as input the time signals obtained with the device and easily classifies different type of signal based on selected features[90]. Future software development can take into consideration convolutional neural network for signal classification.

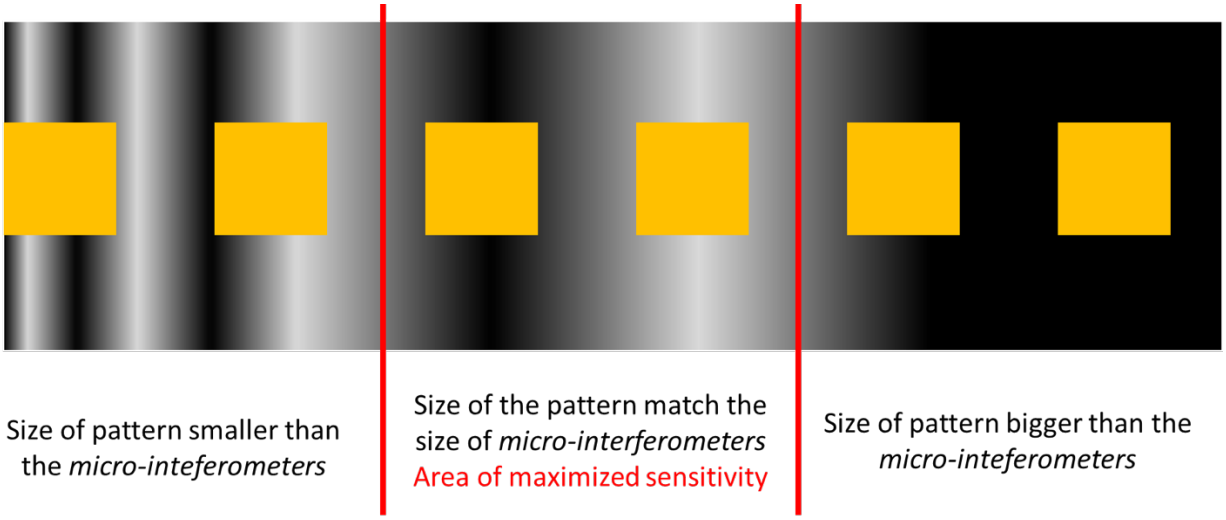

Figure 3.4 Scheme comparing the size of the micro-interferometers with the size of the interference pattern. The yellow squares represent the micro interferometers of 30μm side. The black and white waves represent the interference pattern. Where the size of the local interference wave matches the micro-interferometers size the sensitivity of the device is expected to be maximized.

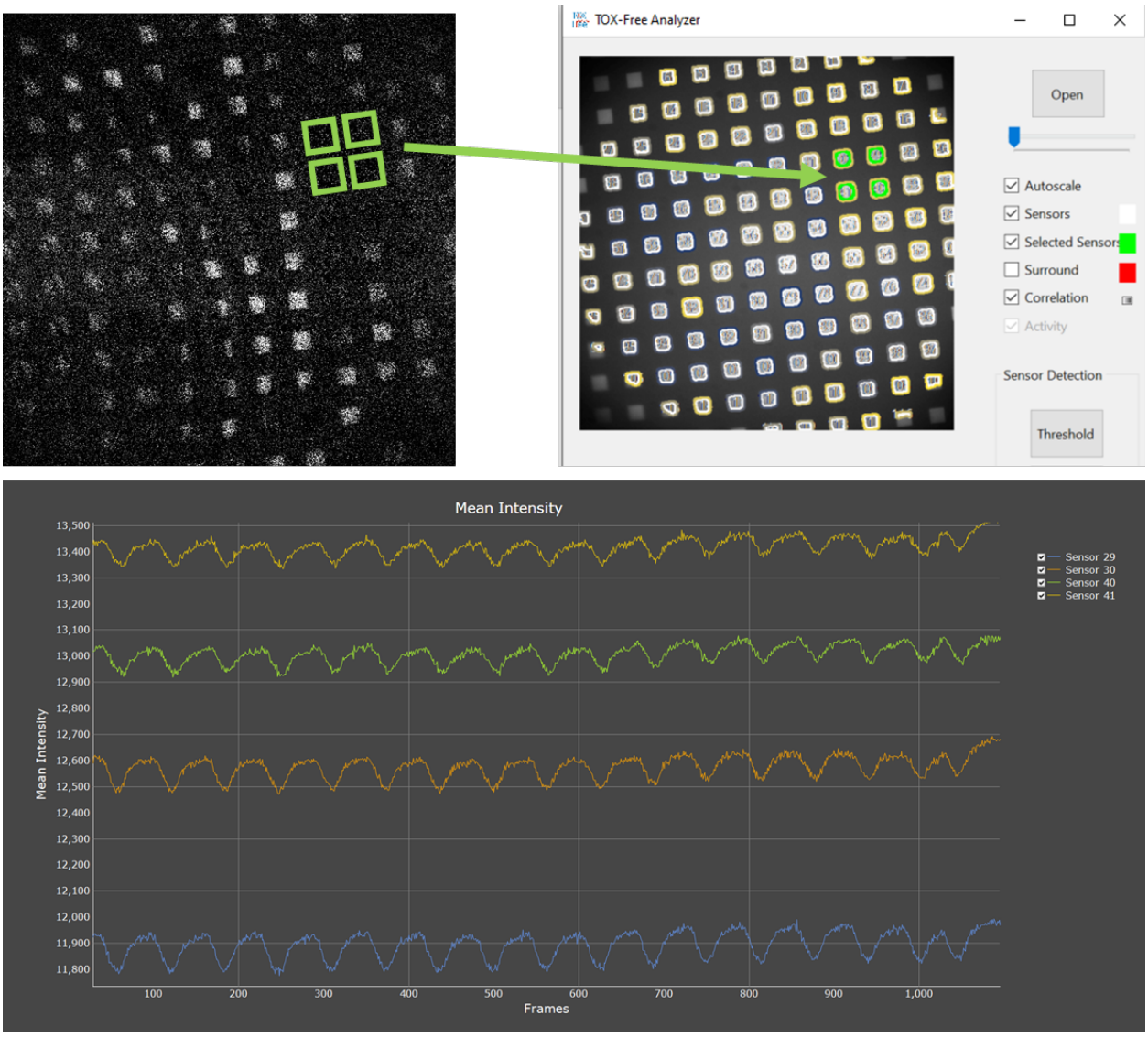

Figure 3.5 Scheme describing the post-processing of the data. a) Fluorescence image after subtracting the first frame from the video. The bottom-left part of the image show interference pattern that is locally smaller than the micro-interferometers. The top-right show interference pattern which size match the micro-interferometer. b) Tox-free software interface showing the same recording where we select the same sensors we indicated in the previous step. c) Fluorescence raw data traces extracted from the 4 selected sensors.

3.4.3 Stimulation and drug response

To further assess the capabilities and versatility of our device, pacing experiments were conducted, where controlled contraction frequencies were induced in hiPSC cardiomyocytes through the application of a voltage stimulus. The pacing involved the administration of controlled electrical stimuli to cultured cardiomyocytes, resulting in rhythmic contractions at specific frequencies. This approach serves as a controlled and reproducible platform for investigating the mechanisms

underlying cardiac arrhythmias and other heart-related disorders[91]. Additionally, the effects of Blebbistatin on contractility amplitude over time following its administration were explored[92]. Blebbistatin, known for decoupling the mechanical contraction of cardiomyocytes from their electrophysiological activity, primarily reduces or halts the mechanical contraction while maintaining electrical activity[93].

In the pacing experiments, a voltage pulsed stimulus was applied between the cis and trans-chambers (Figure 3.1a). Following the recording of a baseline of spontaneous activity, the cell culture was stimulated, achieving a paced contraction frequency of 3Hz with a voltage of 2V and a pulse duration of 200μs (Figure 3.6b). Upon turning off the stimulation, spontaneous beating resumed, and remarkably, this measurement could be replicated several times without causing cell damage or detachment.

Subsequently, 5 μM of Blebbistatin was administered to the cell culture, and the monitoring of cell contractility commenced promptly (Figure 3.6). After 2 minutes, a significant 30% decrease in contractility amplitude was observed. This reduction further reached nearly 70% after 5 minutes. Furthermore, the device demonstrated its capability to detect relevant changes in the contraction profile during drug assessment. For instance, Figure 3.6c displays the averaged contraction shape over a 20-second activity before and after the administration of 5 μM of Blebbistatin. The contraction duration at 50% of the peak amplitude (CD50) was quantified, revealing an increase from 159±47 ms before administration to 213±51 ms after administration.

These results underscore the powerful capabilities of our interferometric biosensor in evaluating the response of hiPSC cardiomyocytes to both controlled pacing and drug administration. The device's precision in pacing contractions and monitoring contractility changes over time provides valuable insights into cardiomyocyte function and drug effects, crucial for advancing our understanding of cardiovascular diseases and the development of effective pharmacological interventions.

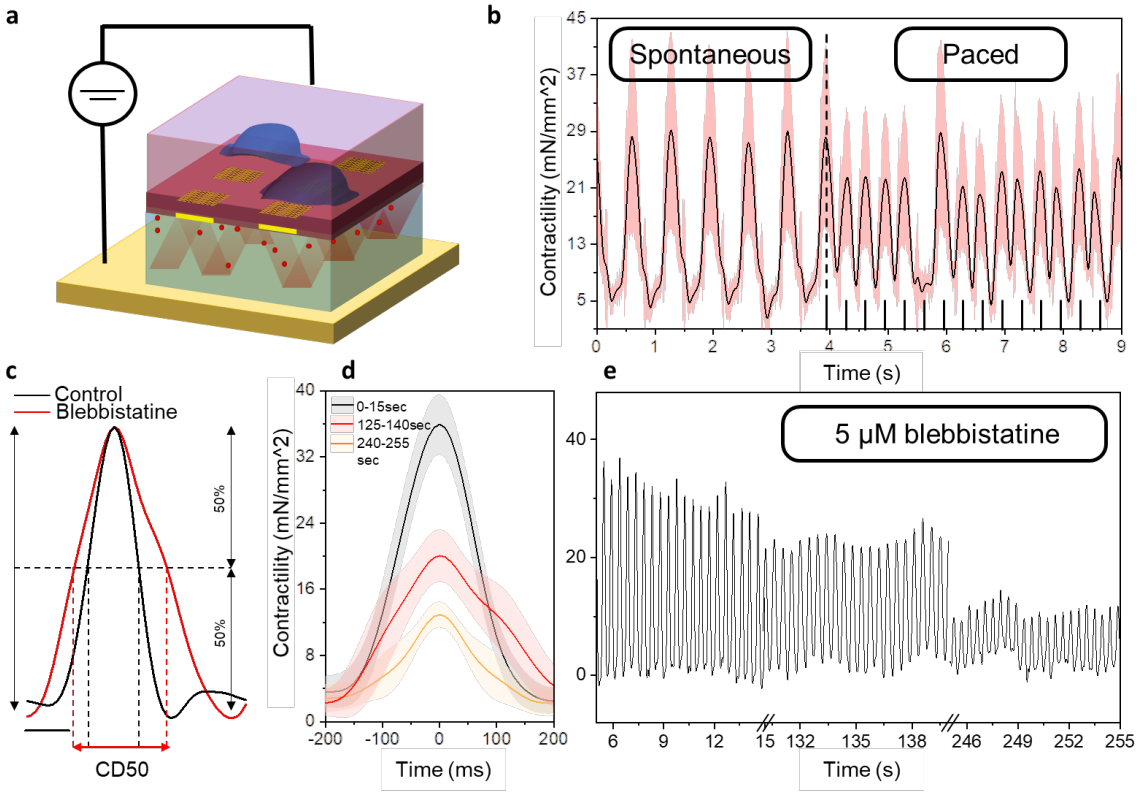

Figure 3.6 Paced and drug detection measures. (a) Scheme the device during paced stimulus configuration. A voltage difference is applied across the cis- and trans-chamber (b) 10 sec of contractility measure over 6 gold micro-interferometer during pacing stimulation (mean ± standard deviation). (c) Normalized averaged contraction traces in drug assessment condition. The black line represents the trace in control condition, the red line represents the contractility trace 2 min after the BB administration. (d) Contractility amplitude for different time interval after the BB administration. (e) Mean contractility recording for 260 sec of after BB administration.

3.5 Device Characterization

3.5.1 Interference Pattern and Optical simulation

To gain insights into the origin of the optical phenomena observed in our device and quantify the contraction forces applied by the cells to the membrane, simulations to study the behavior of the electromagnetic field in the cis-chamber have been performed. Before simulations, a specific experiment was conducted in order to obtain a clear measure of the interference pattern supposed to appear in the optical cavity. In details, a specific sample was designed where both reflecting surfaces were homogeneous. Indeed, the upper surfaces, which is patterned of gold mirror for cell experiments, consisted a single mirror of 2x2 mm. In this configuration a clear and complete image

of the interference patter was obtained. Figure 3.7 shows an image of the interference pattern created in the optical cavity when the fluorescence of the R6G is enhanced. Knowing the parameter of the optical pathway and the camera field of view, the size of the fringes was characterized and measured. Figure 3.7 shows the averaged line profile of the interference pattern in the area highlighted in yellow.

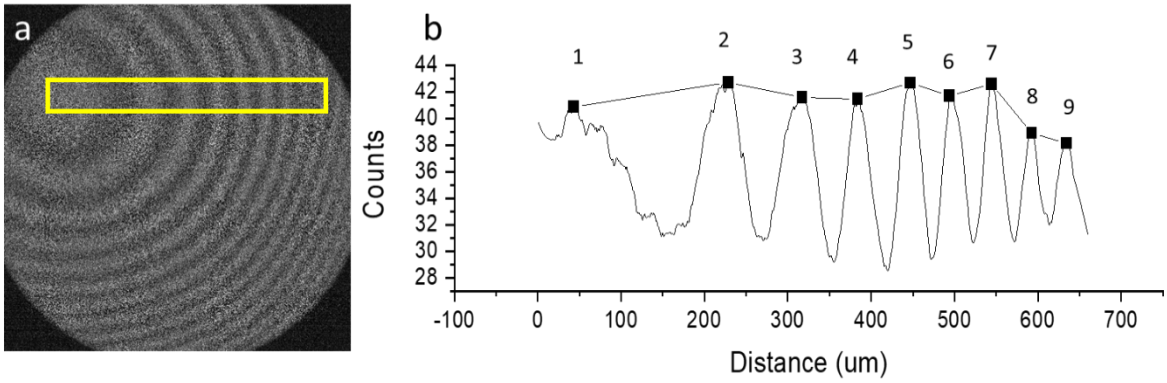

Figure 3.7 a) Image of the interference phenomenon occurring in the homogeneous optical cavity. b) Line profile of the interference pattern.

Thereafter, simulations were conducted to confirm the physical origin of the interference patterns. Figure 3.8b presents a cross-section schematic of the simulation setup. A 2D model of the cis-chamber was designed to reflect the actual sizes and materials of the device. The model consisted of a silicon nitride membrane (L = 500 nm, n = 2.02) covered by a gold layer (H2 = 200 nm). The membrane was separated from the bottom glass (G2 = 500 µm, n = 1.45) by a layer of ethylene glycol (G1 = 15 µm thick, n = 1.43). Additionally, the bottom glass was coated with a thin gold layer (H1 = 20 nm). For the simulation, a dipole source with a wavelength of 592 nm represented the irradiation light, and a virtual monitor was placed at a distance of G3 = 0.5 mm from the bottom glass. Two different simulations were conducted. Firstly, the device in a static condition, where the two surfaces of the cavity were perfectly parallel, resembling the experiment shown inFigure 3.7. Secondly, the scenario in which the membrane bent under the contraction forces applied by the cells was simulated, where the two surfaces no longer remain parallel. To simulate the bending effect, the parameter R was introduced, representing the curvature of the membrane at different levels (R = [50 nm, 100 nm, 150 nm]).

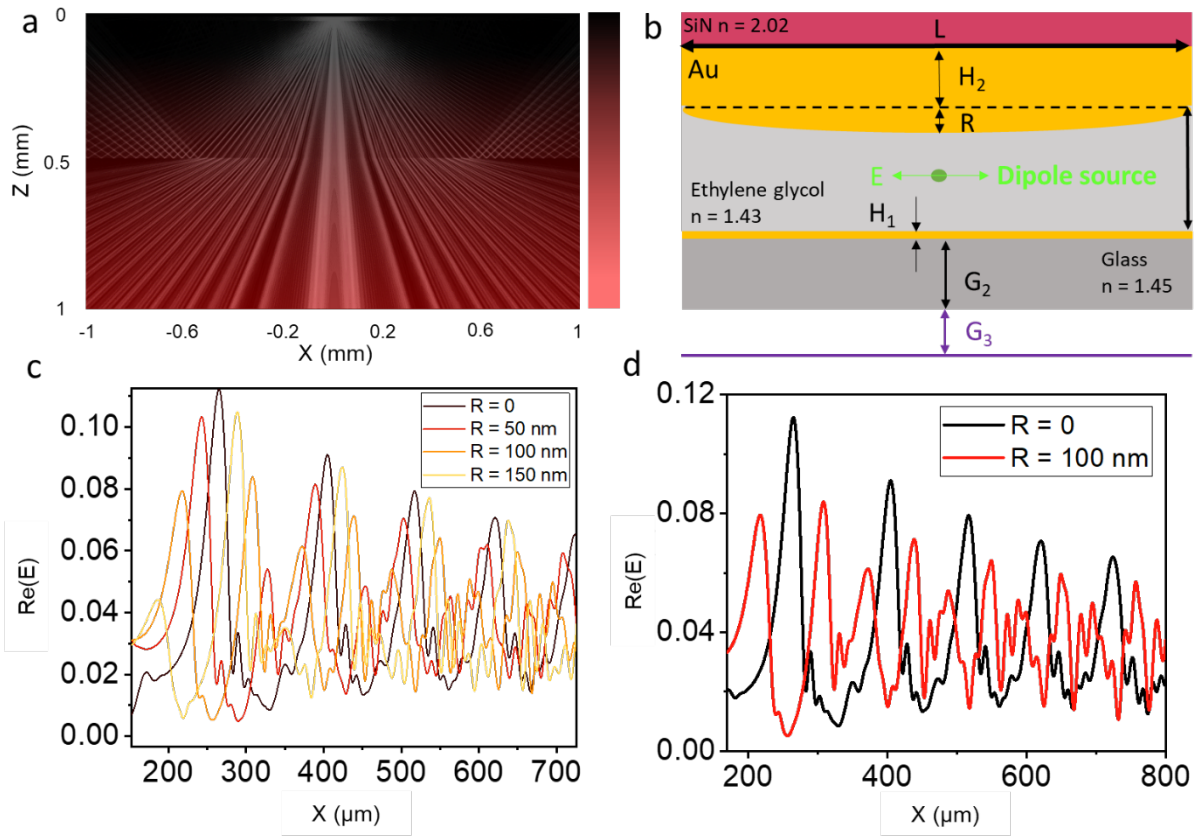

Figure 3.8 Simulation of the optical cavity. A) Electric field interference in the optical cavity. B) Cross section of the simulated optical cavity. C) Interference pattern shift due to membrane bending. D) Interference pattern shift between R=0 and R=100nm.

In the first condition, where the simulation assumes the device is in a static state with the two surfaces of the cis-chamber being perfectly parallel, the results confirm that it is possible to obtain optical interference in the cis-chamber that closely matches the experimental observations (Figure 3.8a). The confirmation of optical interference under the parallel condition offers crucial insights into the underlying physics of our device and assures the accuracy of our contractility measurements. Moreover, in the subsequent analysis, the impact of membrane bending and its influence on the interference patterns was studied. The simulations revealed that as the bending parameter R increased, the phase of the optical interference shifted accordingly (Figure 3.8c). Particular is the behavior of the simulated optical cavity for a displacement R = 100nm: the physical displacement of 100nm forces the optical interference to shift completely out of phase. The interference patterns captured by the virtual monitor exhibited variations that are correlated with the extent of membrane deflection due to the applied contraction.

3.5.2 Mechanical simulations

Afterwards, the dynamic behavior of the silicon nitride membrane was investigated in order to understand the forces that could cause it to bend within the range of displacement observed in the optical phase shift. A finite element analysis (FEA) was performed in COMSOL Multyphisics. A 3D membrane clamped at its edges was simulated immersed in a fluid in order to account for the presence of ethylene glycol Figure 3.9a. The deformation and stress fields across the membrane was simulated for different loading pressure scenarios. The simulations were performed by varying the amplitude (0.1 Pa, 0.3 Pa, and 0.5 Pa) of a quasi-static (2 Hz) pressure load applied on the top membrane face. Figure 3.9b shows the distribution of the maximum deformation of the membrane for an applied load of 0.5 Pa at 2 Hz.

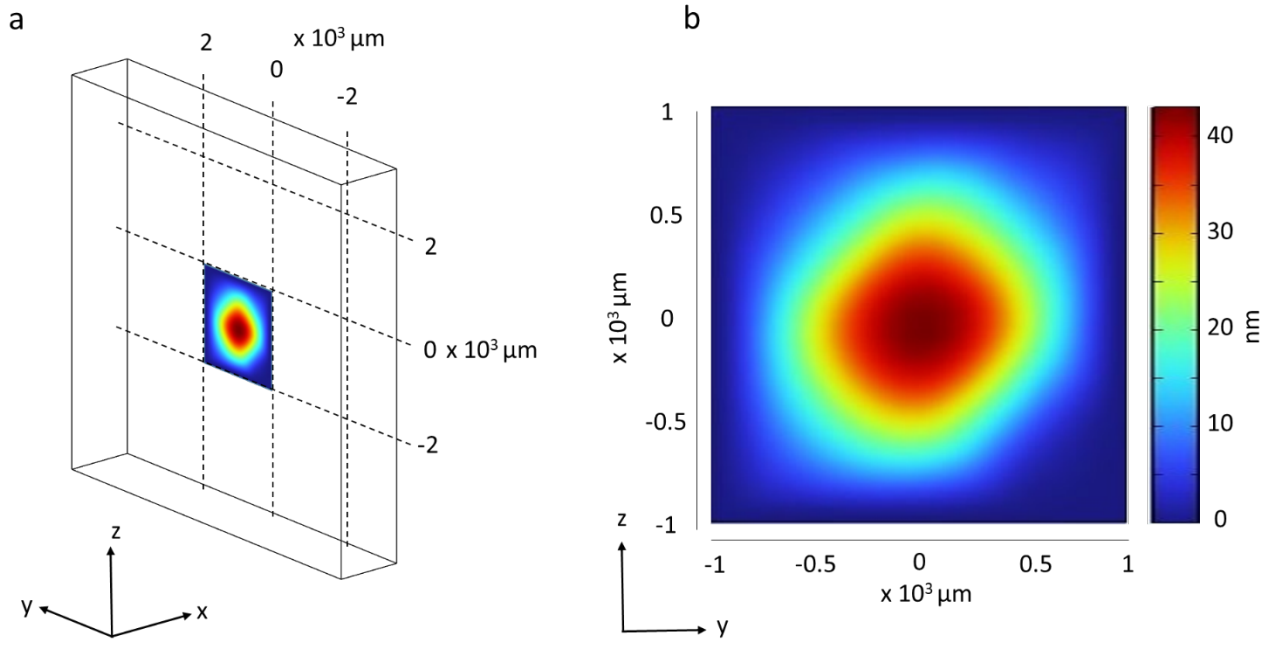

Figure 3.9) Geometry of the thin plate modeled in COMSOL. b) Displacement simulation of the thin plate model under a vertical load equal to 0.5Pa.

The predictions of the numerical simulations have been validated by using the analytical results available in literature. The membrane considered in this study, due to its aspect ratio (L = 2mm, thickness = 500 nm) and elastic properties (E= 250 GPa) can be approximated as a thin plate[94] which dynamic has an upper bound in the membrane-like model and a lower-bound in the thick-plate model (the transition between the two dynamic regimes is dictated by the non-dimensional

parameter $\frac{p}{E}\left(\frac{a}{t}\right)^4$). The validity of both the models which admit closed form solutions under an uniform load was verified [95,96]. Therefore, the match between the analytical and numerical predictions for both these models within the respective range of applicability was verified. As result, the accuracy of the numerical results was validated in the range of material, geometric and pressure parameters of interest for this study, which is intermediate between the two models introduced above but for which, to the best of our knowledge, no closed form solutions are available [97]. The model of the thin plate implies stresses only on the plane of the surface and those stresses are uniform throughout the thickness of the membrane[98]. Due to the smallness of the deformations investigated (with respect to the characteristic dimensions) the membrane behavior is expected to obey the linear elastic regime. The numerical simulations of membrane mechanical deformations show a linear relationship between vertical displacement and traction stress. It predicts, for a quasi-static applied load 0.5Pa, a traction stress and vertical displacement of 40mN/mm^2 and 50nm. These values confirm the validity of the linear elastic model, is the maximum stress is well below the yield stress of silicon nitride, typically within the range 60 -520 MPa. Figure 3.10a shows the temporal relationship between the applied quasi-static pressure load and the resulting maximum vertical membrane displacement (y-axis on the left) and longitudinal traction stress across the membrane (y-axis on the right).

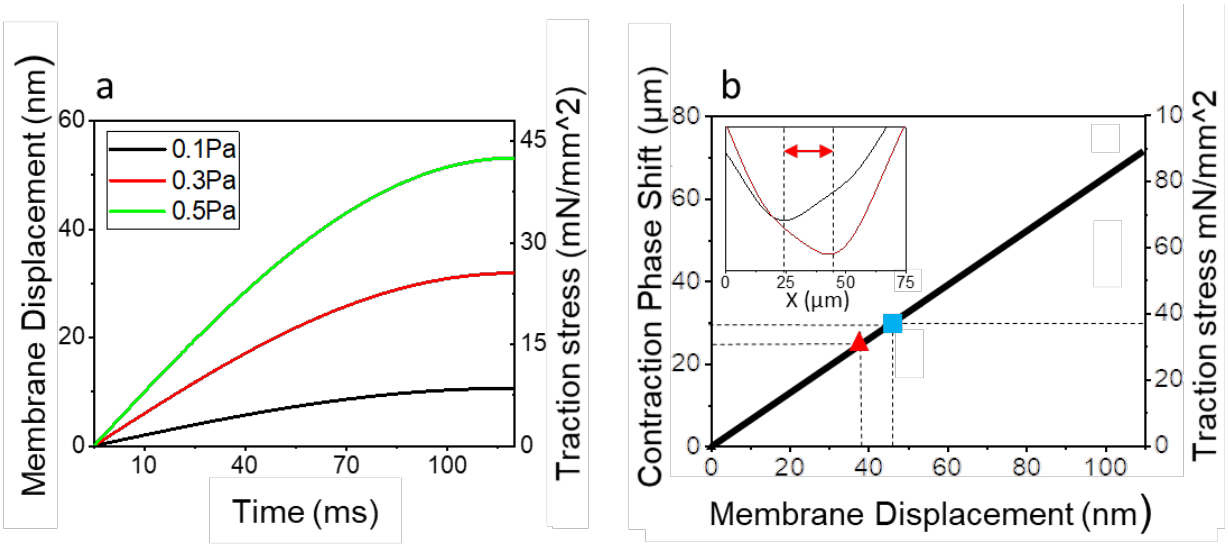

Figure 3.10 a) Mechanical characterization of the silicon nitride membrane. We simulated the membrane displacement under different values of normal load pressure (Pa) and we computed the relative traction

stress along the longitudinal direction (mN/mm^2). The normal load was applied as a 2 Hz sinusoidal pressure with maximum values of 0.1Pa, 0.3Pa, 0.5Pa. b) Shows the linear relationship between the simulated interference phase shift, the simulated membrane displacement and the simulated traction stress during the bending. The blue square highlights the 30µm phase shift that corresponds to the size of the micro-interferometers. The red triangle highlights the experimental phase shift observed on the real device during cardiomyocytes contraction.

In Figure 3.10b, presents a comprehensive graph that establishes the correlation between numerical simulation data and experimental results. The graph showcases the simulation outcomes, demonstrating a linear relationship between the maximum membrane displacement, interference pattern phase shift, and average traction stress experienced during the deformation process (indicated by the black line). The inset shows an example of experimental phase shift during the contraction event that we quantified as 25±5µm. The calculation of the phase shift, both in the simulated and experimental datasets, involved determining the spatial difference (µm) between the negative peak values of the interference line profile. The red triangle on the graph indicates the actual experimental phase shift data point, effectively placed along the characteristic line predicted by the simulations. Furthermore, the blue square indicates the anticipated membrane displacement, and consequently, the expected traction stress, corresponding to a phase shift of 30µm, which aligns with the actual size of our gold *micro-interferometers*.

3.6 Conclusion and Perspective

The results presented in this chapter demonstrate the successful development and application of an interferometric biosensor for high-sensitive and label-free recording of hiPSC cardiomyocyte contraction in vitro. The capture of CMs beating frequency and the quantification of contractile forces exerted by the CMs monolayer were achieved by the device. Averaged contractility of 34±4 mN/mm2 at 13 DIVs was quantified, aligning with the state-of-the-art literature (https://innovitro.de/wp-content/uploads/2021/10/210911-innoVitro-Contractile-Force-Flyer.pdf). The device proved capable of accurately detecting and quantifying forces applied during paced contractions and notably discriminating variations in contractility during drug assessment. The key element facilitating these outcomes is the design of an optical cavity whose parameters are modified by CMs contraction. The technology detects displacements on the order of tens of nanometers, enabling the use of thin silicon-based membranes as a flexible substrate,

despite their high Young's modulus[91,99]. Silicon-based materials, standard in micro- and nano-fabrication, offer an advantage for scaling up the fabrication process toward high throughput[37,54]. Crucially, the silicon-based micro-interferometers are the same size as the CMs, providing a spatial resolution at the single-cell level. While the current device measures contractility across the entire CMs monolayer, future enhancements may lead to a single-cell resolution contractility measure of the CMs monolayer. Importantly, unlike many polymeric-based devices, our biosensor enables the simultaneous measurement of contraction and imaging of the cell culture, as the nanometric range displacement of the silicon nitride membrane does not significantly affect the optical focus of the objective. In this work, 900 micro-interferometers uniformly distributed on the 2x2mm^2 membrane were employed to ensure that the interference pattern's period in a sub-area of the device would match the micro-interferometer size, ensuring reliable and repeatable detection of CMs contraction. While the optimal working area's location may vary among different devices due to the practical triviality of perfect cavity interface alignment (see chapter 3.4.2), we consistently obtain a substantial number of micro-interferometers (around 50) operating in the area where the interference pattern's period matches the micro-interferometers' size, maximizing sensitivity (n = 9). The signals from micro-interferometers in this sensitive area are averaged to obtain a robust measure of membrane displacement. One limitation of the proposed approach is that flexible and extracellular matrix-like substrates are typically favored for better mimicking physiological mechanical stimuli in the cell environment[55,62]. However, the combination of flexible materials like PDMS with a silicon-based substrate and appropriate fabrication processes can lead to a new family of devices providing the necessary mechanical stimulus and properties for both cell development and high-resolution contractility measures. Toward this goal, micro-interferometer parameters, including size, reflectivity, and refractive index, can be optimized and modified. Different excitation wavelengths, solvents, and fluorescent molecules can be explored to obtain interferences suitable for single-cell detection.

4 Contractility Assessment in CMs Monolayer at Single Cell Resolution

4.1 Significance

4.1.1 Beyond the monolithic approach

Understanding latent cardiomyocyte heterogeneity in both healthy and failing organs is crucial, yet current single-cell approaches face significant limitations[100]. The prevailing perspective characterizes cardiomyocytes as a homogenous population of cells with a single phenotype, overlooking the intricate diversity that exists[101]. The major obstacle lies in the time-intensive nature of current techniques for studying single-cell cardiomyocytes, since viable cells have a limited lifespan of hours, single cell technique allows to measure no more than five cell from the same batch[100]. This temporal constraint results in the study of only a few cells from each preparation, leading to a substantial waste of remaining cells. This not only poses ethical concerns but also creates financial and personnel challenges. The low number of cells assayed, coupled with the necessity to amalgamate measurements from various myocyte preparations, raises questions about the statistical power of these studies to test hypotheses effectively. To address these issues, there is a compelling need to accelerate measurements and assess numerous cells in parallel, potentially revitalizing the feasibility of single-cell studies[102].

While force transducers and soft strain gauge sensors have been developed, they grapple with significant spatial resolution limitations. Overcoming these challenges is pivotal to unlocking a more comprehensive understanding of cardiomyocyte behavior, allowing for a nuanced exploration of their heterogeneity in diverse physiological and pathological conditions.

4.1.2 Contraction Propagation

It is well-established that the ability of contraction propagation in the heart may be affected by various cardiac diseases, including arrhythmias, cardiomyopathies, and ion channelopathies. These conditions can have significant implications for patient health and may require medical intervention to manage symptoms and reduce the risk of complications[50,103]. Cardiac arrhythmias associated with abnormal heart contraction propagation include various conditions that result in

irregular heartbeats or disturbances in the heart's electrical signals. Some examples of cardiac arrhythmias linked to abnormal heart contraction propagation are:

Atrial/Ventricular Fibrillation (AF/VF) AF/VF is a common arrhythmia characterized by rapid, irregular electrical activity in the atria, leading to ineffective atrial contraction and potential blood stasis, which can increase the risk of stroke.

Ventricular Tachycardia (VT): VT is a fast, regular heart rhythm that originates in the ventricles and can lead to hemodynamic compromise and degenerate into VF.

Atrial Flutter: Atrial flutter is a rapid, regular atrial arrhythmia that can lead to palpitations and is associated with an increased risk of stroke.

Supraventricular Tachycardia (SVT): SVT is a broad term for various rapid heart rhythms that originate above the ventricles and can cause symptoms such as palpitations, dizziness, and chest pain.

The relationship between cardiomyocyte coupling and arrhythmogenesis has been studied extensively. Alterations in gap junction organization and connexin expression, which mediate myocyte-to-myocyte electrical coupling and communication, have been identified as a common feature of human heart disease conditions with an arrhythmic tendency[18].The idea that such changes may contribute to the development of a pro-arrhythmic substrate in the diseased heart has gained ground over the last decade. Therefore, the detection of alterations in conduction/coupling among cardiomyocytes is crucial, as it can provide valuable insights into the propagation of contraction and the development of arrhythmias in acute and chronic heart disease[18]. Furthermore, cardiac electrical signal propagation involves factors **internal to the cardiomyocyte** and contributors from neighboring cells[104]. Further research and clinical studies are needed to better understand the full scope of diseases related to impaired contraction propagation in the heart.

From a general point of view, if the contraction propagation is impaired, different region of the cardiac tissue will show differences in contraction timing and/or properties, like contraction strength[105]. Those malfunctions can be modeled in vitro by using for instance hiPSC cardiomyocyte monolayers. To study dysfunction to the contraction propagation and the effect on the ability to generate forces of the cardiac tissue in vitro we need the proper technology. In detail,

a technology able to measure different regions of a CMs tissue independently, synchronously, at high frequency is still needed.

4.2 Device concept

The device presented in this section can be defined as a "single cell resolution" version of the one presented in Chapter 3. With the idea to obtain a sensor which could monitor simultaneously and independently different areas of the same cardiac monolayer, we realized a device that interfaces the cells with a substrate made two different materials, with very different level of stiffness. The first material, Silicon Nitride (0.5 and 1 um thick) works as a rigid substrate, consisting in the structural bone of the device. The second, PDMS which stiffness is 4 order of magnitude lower that SiN, positioned in well-defined zone of the device, is the active part of the device. The difference in stiffness between the two materials allows to obtain a rigid substrate which can be deformed only in the engineered areas made of PDMS, namely the independent *micro-interferometers*.

The device technology, described in Figure 4.1, is based on the same concept of the *micro-interferometers* described in the previous chapter. In the previous device each *micro-interferometer* was part of a single sensor, averaging the contraction signal generated by the whole cardiomyocyte monolayer. Differently, the device was developed realizing PDMS windows with 30um diameter in the SiN substrate, as shown in Figure 4.1. The PDMS window is highly flexible and free to oscillate, while the SiN is fixed. Notably, the thin PDMS layer cover the whole device, guarantying an optimal adhesion layer for cardiomyocytes. The PDMS windows, namely the single cell micro-interfermoters, were realized in the whole silicon nitride membrane that was patterned with 50um pitch (Figure 4.1b). When cardiomyocytes contract the PDMS window is deformed consistently with the contraction of the single cell that is above. In this way, if differences in contractility properties occurs in different cells of the monolayer, each interferometer will be deformed consistently, resembling the difference in contraction. The deformation occurring in each independent *micro-intererometer*, is detected using the same concept explained in section 3.2. Briefly, a variation of the distance between the two reflecting surface defining the optical cavity of the *micro-interferometers* changes the intensity of the fluorescence interference which is reflected and acquired with the camera.

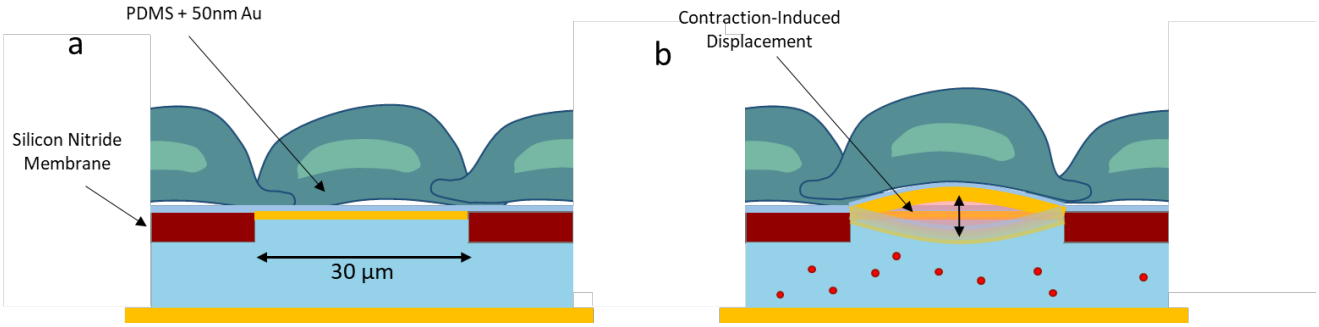

Figure 4.1 Scheme of single cell micro interferometer. a) It shows a static scheme of the single cell micro interferometer; each PDMS window is 30µm of diameter and it is 1-2 µm thick. b) Scheme of the contraction-induced displacement of the PDMS layer.

The cis-chamber, defining space between the interfaces, is filled with a fluorescent molecule (rhodamine, R6G, 0.2 mg/ml) dissolved in a non-volatile liquid (ethylene-glycol). As shown in Figure 4.1b, when irradiated by the correct wavelength light enhancing fluorescence emission of R6G (λ_{ex} = 543/22 nm). While theoretically an interference patter can be created as previously described, the fluorescence signal belonging to the volume under each PDMS mirror is independent and thus the formation of the pattern is very unluckily. During the cell contraction, each PDMS mirror behaves as the oscillating part of an interferometer, in which the distance *l* changes (inset Figure 3.1a). As a result, the optical signal derived from each *micro-interferometer* changes according to the part of the tissue located above it. When the cells contraction ends, the membranes return to its original configuration and, consequently, the signals are restored to the reference value. During measurements the fluorescence intensity is acquired simultaneously from different sensor as a shown in Figure 4.2a. Figure 4.2c show an example of a trace derived from a single independent *micro-interferometers*.

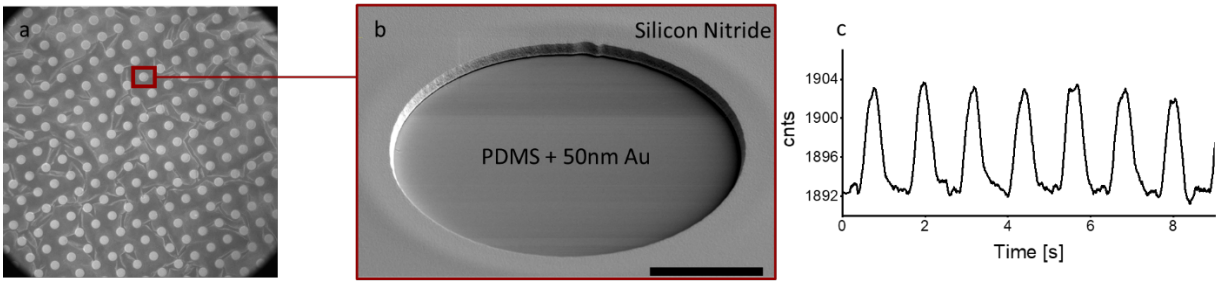

Figure 4.2 a) Optical image of the single cell resolution device. b) SEM image of the PDMS window surrounded by the silicon nitride substrate. Each window has a diameter of 30 µm. c) Example of contraction signal coming from a single cell micro-interferometer.

4.3 Results

4.3.1 Device Optimization

To determine the optimal device configuration, several tests were conducted, with the main goal being the selection of the most suitable thickness for the flexible polymeric window, considering both achieving the best signal-to-noise ratio (S/N) and ensuring a feasible fabrication process. In essence, the PDMS windows were created by dry etching the Silicon Nitride in defined regions. The etching process employs gas that selectively removes different materials, in this case, Silicon Nitride. This process typically concludes when the material is entirely etched. In our process, a resist mask outlines the areas with a diameter of 30 µm where the Silicon Nitride needs to be removed (Figure 4.3). On the opposite side of the resist, the gold-PDMS layer was previously deposited. During the etching process, the Silicon Nitride is removed at a rate of 1 nm/sec. The etching process must cease when the Silicon Nitride is completely removed, preventing damage to the gold-PDMS layer or breakage.

The thickness of the Silicon Nitride can be roughly monitored by its color, but the optimal thickness for our device remained unclear. Therefore, in the initial stage, different Silicon Nitride thicknesses were tested: 250 nm, 100 nm, 50 nm, and 0 nm (sample where the Silicon Nitride was completely removed). While it is evident from an S/N perspective that the thicker the Silicon Nitride, the lower the S/N, concerns about the device's robustness persisted. Indeed, before measurement, the device needs to be coated with cell tissue and incubated for at least 10 days, being subjected to biological forces such as cardiomyocyte contraction. Therefore, the primary concern is its structural integrity to withstand these forces without breaking.

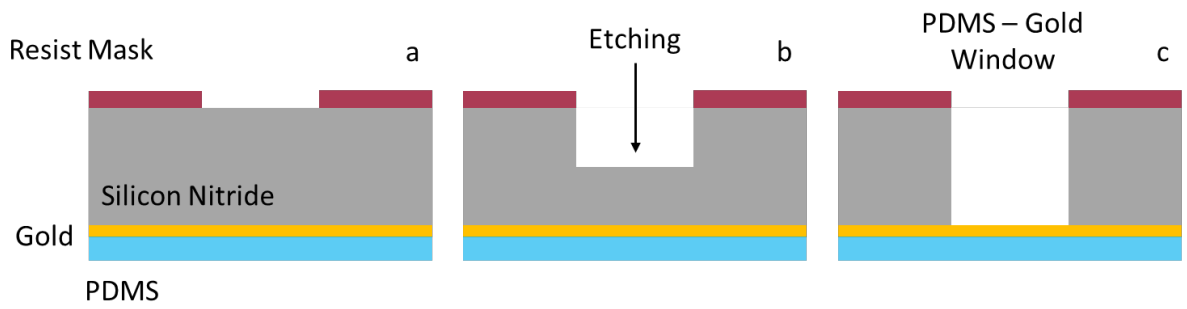

Figure 4.3 Etching process of silicon nitride until the formation of gold-PDMS window. The PDMS layer is 1-2 µm thick, depending on fabrication parameters.

The four device configurations were tested by cultivating hiPSC cardiomyocytes on the device and incubated for 9 DIVs. After the maturation of cardiomyocytes spontaneous recording of contraction were conducted. Figure 4.4 shows an example of the signal of contraction obtained from the different devices with different silicon nitride thickness. The configuration where the silicon nitride was completely removed, and thus, the oscillating interface only consist of PDMS and gold show the best S/N ratio. Furthermore, the obtained signal is similar in shape to the one showed in the previous chapter and in literature.

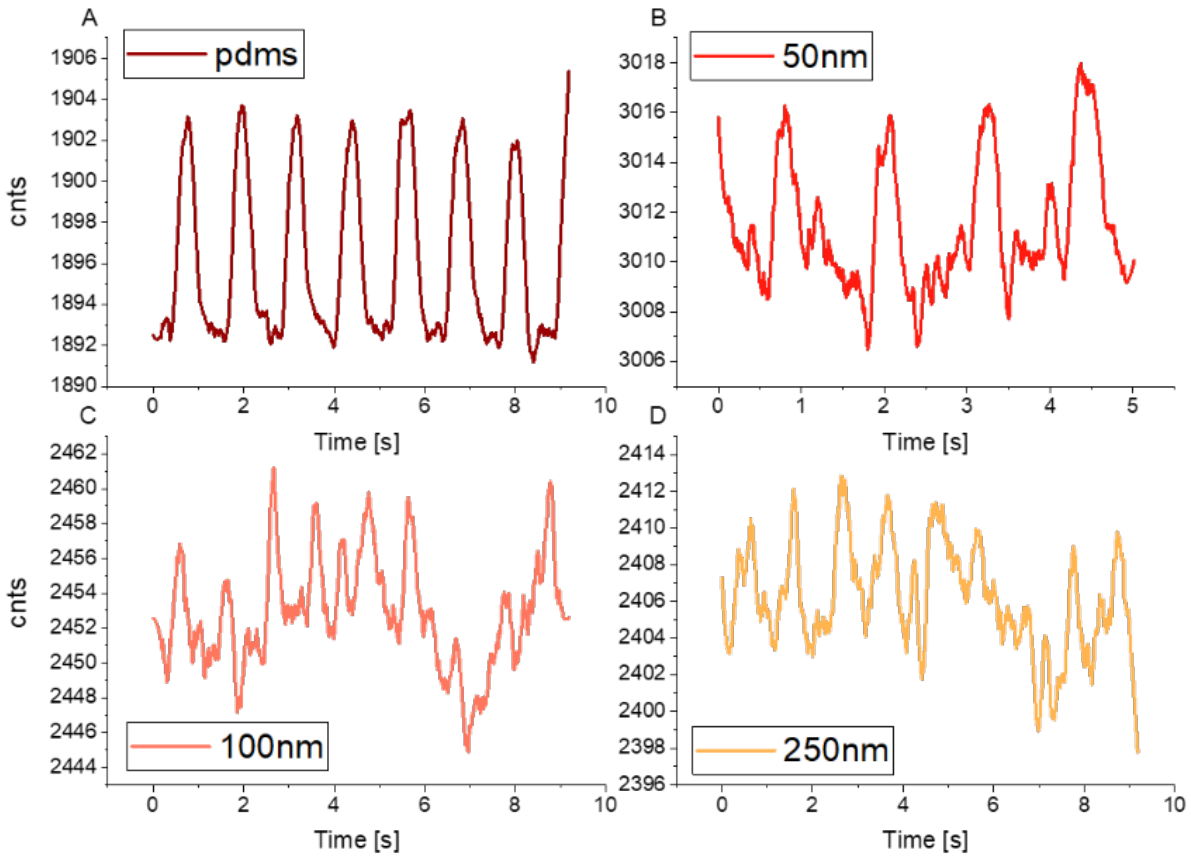

Figure 4.4 Signals coming from different device with different thickness of silicon nitride.

The S/N was computed among signals from 4 devices confirming a significant differences between the device where the active part of the device is only made of PDMS and gold versus the devices with a thin layer of silicon nitride. Furthermore, the device only made of PDMS and gold successfully survived to experimental measure in 100% of the trials. This also suggest there is space for improving the flexibility of our polymeric interface, improving the S/N without impairing the robustness.

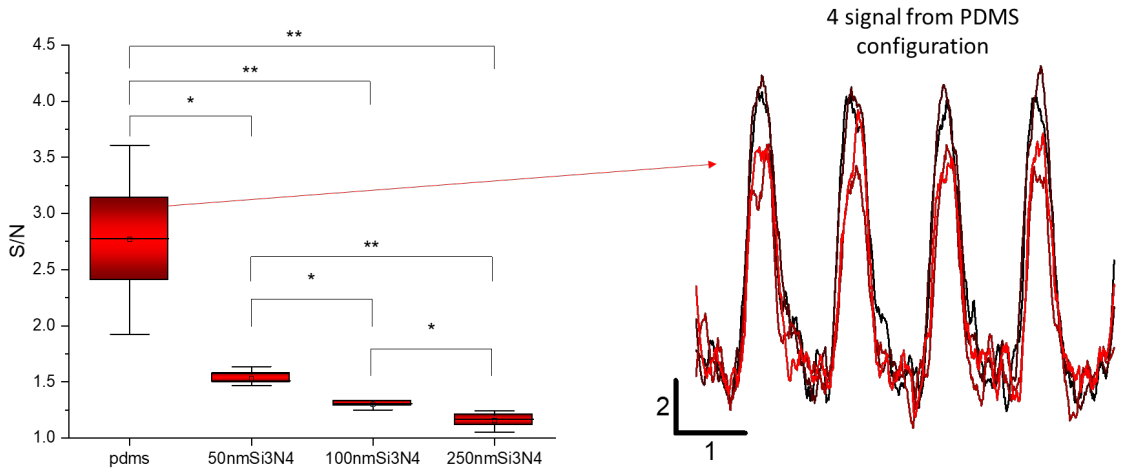

*Figure 4.5 S/N measured across the four different thickness of the device. The trend confirms that the thinner the silicon nitride the better is the quality of the signal. Where the silicon nitride is completely removed and the oscillating part of the sensor only consist of PDMS the S/N is double. Kruskal-Wallis, **p<0.01, *p<0.05.*

4.3.2 Contraction propagation

In our preliminary assessments, our device demonstrated the capability to temporally discern the initiation of contraction in a 2D monolayer of hiPSC cardiomyocytes. Three contraction signals from distinct micro-interferometers on the same device, positioned in various areas as depicted in Figure 4.6b, are presented in Figure 4.6a The device acquires temporally independent signals of contractility from the different interferometers. Consequently, a notable delay in contraction timing was observed among four closely positioned interferometers in two different areas of the device. A contraction delay of 50 ms was measured among different areas of the device at a distance of 350 µm, aligning with existing literature findings[36].

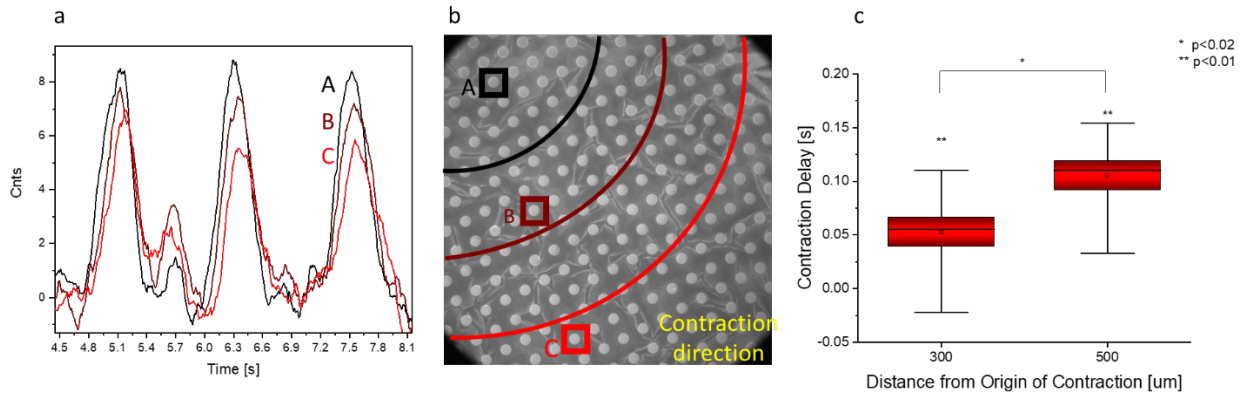

Figure 4.6 Measurement at single cell resolution. a) The graph shows the signal from 3 different sensor in different position of the device. b) Position of the different sensors. c) Statistic of contraction delay among 4 sensors in position B and C (A is considered the origin of the contraction). Kruskal-Wallis non-parametric test.

4.4 Methods

4.4.1 Fabrication

The silicon nitride membrane was fabricated from a double-sided silicon nitride-coated wafer, following the procedures outlined in previous studies. Each individual membrane possesses a 2x2 mm^2 area and is situated within a silicon frame of 2x2 cm^2 (Figure 4.7). For this device configuration, the membrane thickness was tested within the range of 0.5 µm to 1 µm. The initial cleaning process involved immersing the sample in a piranha solution (3:1 sulfuric acid and hydrogen peroxide). After an overnight soak in Milli-Q water, the first lithographic process ensued. A specific mask, featuring a matrix of circles with a 30µm diameter and 50µm pitch, was designed (Figure 4.7- a1). S1813 microdeposit resist was spun onto the hollow part of the membrane at 4000rpm for 1 minute. Subsequently, a 3-minute soft bake process solidified the resist. A 15-second exposure was conducted through the membrane by flipping the sample, exposing the flat part to direct UV lamp radiation. The high transparency of SiN allowed the UV radiation to imprint the resist on the opposite side, and the thinness of the membrane (500-1000 nm) did not compromise the lithography quality. Following a 45-second development in MF319, a plasma oxygen treatment (100W, 120 seconds, 100% O2) cleaned the developer and residual resist. A thin layer of 5nm Ti and 50nm Au was then deposited by an e-beam evaporator (Figure 4.7– a2). A subsequent lift-off process removed the excess metal, resulting in a matrix of reflective

circle-shaped mirrors on the membrane (Figure 4.7– a3). On the side where the mirror matrix was deposited, a thin layer of PDMS was applied (Figure 4.7– a4). A 1:20 dilution of PDMS Sylgard was spun for 10 minutes at 5000rpm and baked at 65 °C for 3 hours. Following this, an image reversal resist (AZ5214) was spun on the flat surface and baked at 112°C for 1 minute. Exposure was conducted through the membrane by flipping the sample to face the gold mirror to the UV lamp. In this case, no mask was required, as the mirror matrix acted as a natural mask, creating a mirrored pattern on the opposite side of the membrane. After a 45-second development in AZ726, the resist served as a mask for the RIE-ICP process, removing the SiN. A specific recipe was fine-tuned to cease etching the SiN after its complete removal in the region defined by the resist mask. The result yielded small (30µm) circular PDMS membranes coated with a thin layer of gold. The SiN surrounding the matrix of PDMS membranes functioned as the rigid substrate for the device.

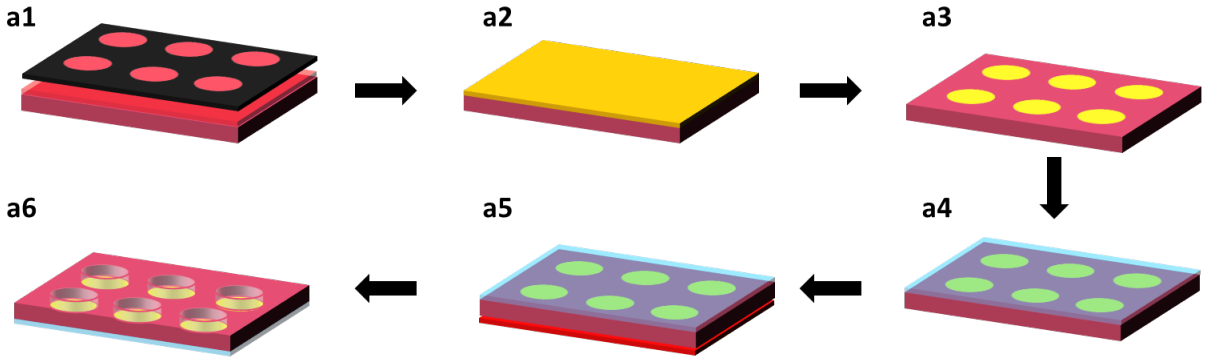

Figure 4.7 Fabrication process of single cell PDMS micro membrane interferometers.

4.4.2 Experimental set up

In this study, we employed an inverted microscope (Nikon Eclipse Ti2) equipped with a TRITC fluorescence filter cube set (Nikon: excitation wavelength λex = 543/22 nm, emission wavelength λem = 591.5/43 nm) as our experimental setup. Fluorescence excitation was achieved using a LED light source (pE-300lite, CoolLed). The system utilized long working distance objectives (Nikon 20×/0.45 and Nikon 60×/0.70) for focusing and collecting both exciting light and fluorescence. To capture the output fluorescence, a CMOS camera (Photometrics-Kinetics) with 10.24-megapixel resolution, binning capability up to 4×, and high sensitivity and speed capabilities (up to 498 frames per second across the entire field of view fullframe) was integrated into the setup. The CMOS camera was controlled by a computer equipped with Micro Manager 2.0 software.

Additionally, a halogen lamp above the microscope was incorporated to aid in sample observation in transmission mode.

HiPS-CM (iCell cardiomyocytes) were procured from FUJIFILM Cellular Dynamics, Inc. (FCDI). Prior to cell seeding, the devices underwent sterilization with 30 minutes of ultraviolet exposure and were subsequently coated with 50 µg/ml fibronectin (Roche Applied Science) for 1 hour at 37°C, 5% CO2 in a humidified incubator. iCell cardiomyocytes were directly seeded on the devices at a density of 10,000 cells per device and cultivated according to the specifications of the commercial supplier. Recording of cardiomyocyte contractions commenced from 8 days post-plating.

The data obtained in this study consisted of video recordings in .tif format. These .tif files were analyzed using Tox-FREE software (cite). The results generated by the software were saved in .csv format and subsequently imported into OriginPro 2020a (OriginLab) for further data analysis.

4.5 Future Perspective

A series of experiments will push the boundaries of our current knowledge on drug testing and toxicity assessment in the context of heart tissue. Our immediate focus lies in conducting experiments to showcase the capability of the single-cell device in detecting drug toxicity within the intricate milieu of the cell environment. By subjecting cardiomyocytes to a diverse range of pharmaceutical agents, we will decipher the responses at the single-cell level. The upcoming experiments are poised to underline the significance of analyzing drug effects at the single-cell level. Traditional approaches often mask the individual variations within a tissue, but our device allows us to dissect the responses with unprecedented precision. Beyond drug-specific assessments, our experiments will shed light on the general malfunctions within heart tissue. By examining the single-cell responses collectively, we aim to identify patterns and irregularities that may indicate broader issues in tissue function. This holistic perspective will contribute to a deeper comprehension of cardiac physiology and pathophysiology. Looking further into the future, we envision integrating our single-cell device with cutting-edge technologies. This amalgamation could include artificial intelligence for data analysis, microfluidic systems for precise drug delivery, and advanced imaging techniques for real-time monitoring. Such integration will enhance the capabilities of our device and propel cardiac research into new dimensions.

The future of cardiac research with our single-cell device holds exciting prospects. Through meticulous experiments, we aspire to contribute valuable insights into drug toxicity, unravel the intricacies of single-cell responses, and advance the field of cardiology towards more personalized and effective therapeutic strategies.

4.6 Discussion and Conclusion

While both heart failure and cardiomyopathies exhibit altered contractility, existing treatments do not address this directly. The pivotal role of modified contractility in these conditions has spurred ongoing efforts to create compounds that directly influence it. Inotropes like dobutamine and milrinone enhance contractility and intracellular calcium levels, raising the risk of adverse outcomes. Typically reserved for palliative care or temporary support, these drugs may precede ventricular assist devices or cardiac transplantation. A recent focus involves myotropes, substances designed to impact sarcomeric machinery and modify contractility without affecting intracellular calcium levels[106]. The development of such molecules to address cardiac contractility requires novel devices that can assess their performance and effectiveness in vitro before they undergo in vivo and clinical trials. The device presented in this chapter attempts to satisfy this need by providing an effective in vitro platform to study molecules' effects on cardiac contractility.

The development of a device able to discriminate single-cell contribution to cardiac contraction opens avenues for addressing several critical aspects in the field of cardiac research. First, the ability to monitor individual cardiomyocytes provides a platform for unraveling the heterogeneity within a cell population[53,100]. This is particularly relevant in understanding how variations in cellular behavior contribute to overall tissue contraction and function. Nonetheless, the device's capacity to capture label-free contractility in hiPSC cardiomyocytes positions it as a potent tool for disease modeling. By applying this technology to cells with specific genetic mutations or disease conditions, it is possible to gain insights into the mechanical consequences of various cardiac disorders. The high sensitivity and versatility of the device enhance its utility in drug assessment studies. The real-time monitoring of contractility changes in response to pharmacological agents provides a more comprehensive understanding of drug effects on cardiac function. Looking ahead, future iterations of the device could explore enhancements such integrating multi-modal capabilities. In detail, the combination of this technology with

electrophysiological recording techniques such as calcium imaging could enhance our understanding on the correlation between action potential and contraction propagation. Additionally, advancements in material science may lead to improvements in substrate properties, further refining the physiological relevance of the experimental setup. Finally, the development of this device opens avenues for collaboration between engineers, biologists, and clinicians. Its applicability across disciplines fosters a holistic approach to cardiac research, with potential implications for diagnostics and therapeutic interventions.

In summary, the single-cell device presented in this chapter represents a pioneering contribution to the field of cardiac research. Its capabilities, combined with the insights gained from its application, mark a significant step forward in understanding the intricacies of cardiomyocyte contraction. As this technology continues to evolve, it holds promise for advancing our knowledge of cardiovascular physiology and pathology.

5 Conclusion

In this thesis I presented a novel device for cardiac contraction measurement in vitro of whole culture and at single cell resolution. I developed and applied an interferometric biosensor, showcasing its high sensitivity and label-free recording capabilities for monitoring the contraction of hiPSC-CMs in vitro. The device, equipped with over 900 micro-interferometers distributed on a 2x2mm^2 membrane, has proven its capacity to detect displacements on the order of tens of nanometers, enabling the quantification of contractile forces exerted by hiPSC-CMs monolayers. The experiments have not only validated the feasibility of assessing contractility in hiPSC-CMs but have also demonstrated the device's ability to discriminate variations in contractility during drug assessments. The averaged contractility of hiPSC-CMs monolayers, quantified at 34±4 mN/mm2 at 13 days post-plating, aligns with state-of-the-art literature, affirming the device's reliability and relevance in the field[53]. Furthermore, the device's design, incorporating a silicon-based membrane and micro-interferometers that match the size of individual CMs, ensures spatial resolution at the single-cell level. This is a remarkable advancement, providing a level of detail and sensitivity previously unattainable in traditional methods.

The interferometric technology showcased in this thesis offers a unique opportunity for precise measurement of displacement, which extends beyond its application in cardiac research. The capability to detect nanometer-scale displacements with high sensitivity has broad implications for various fields and applications where accurate measurements of displacement are essential[107]. For instance, in the field of material science and engineering, the interferometric technology could be employed to assess mechanical properties, such as elasticity and stiffness, of different materials and structures[108]. This could aid in the development of advanced materials with tailored properties for specific applications, ranging from aerospace engineering to biomedical devices. Moreover, in the realm of nanotechnology and semiconductor manufacturing, the ability to precisely measure displacements at the nanoscale could enhance the fabrication process of microelectromechanical systems (MEMS) and nanoelectromechanical systems (NEMS)[109]. Furthermore, in biomedical research and diagnostics, the high sensitivity and precision of interferometric measurements could facilitate the development of novel diagnostic tools and sensors for detecting biomolecular interactions, cellular responses, and disease markers with unprecedented accuracy[110]. Overall, the transferability of interferometric technology to other applications and fields holds great promise

for advancing scientific research, technological innovation, and practical applications across diverse domains. Through interdisciplinary collaboration and continued refinement, this technology has the potential to drive significant advancements in various fields requiring precise displacement measurements.

The technology's ability to simultaneously measure contraction and image the cell culture is a notable feature, enhancing its utility in studying cardiac tissues with a comprehensive approach. For instance, the thesis opens new avenues for studying the correlation between action potential and contraction in cardiomyocytes. By combining the single-cell device with electrophysiological optical measurements, such as calcium imaging, the intricate relationship between electrical activity and mechanical function in cardiac tissue can be investigated. This holistic approach promises to deepen our understanding of cardiac physiology and pathology, paving the way for more targeted therapies and interventions for cardiovascular diseases. In addition to its direct applications in cardiac research, the potential of this device can be further enhanced by integrating artificial intelligence (AI) for image processing of the results. By leveraging AI algorithms, researchers can extract valuable insights from the optical signals of contraction recorded by the device. AI-powered image processing techniques can analyze the subtle changes in cell morphology and contractile behavior, providing quantitative measurements with high accuracy and efficiency. Moreover, AI can play a crucial role in analyzing calcium imaging data to investigate the action potential dynamics in cardiomyocytes. By correlating the optical signals of contraction with calcium transient signals, AI algorithms can unravel the intricate relationship between electrical excitation and mechanical contraction in cardiac tissue. This integrated approach offers a comprehensive understanding of the electrophysiological and mechanical properties of cardiomyocytes, shedding light on the underlying mechanisms of cardiac function and dysfunction. Overall, the synergy between the novel device presented in this thesis and AI-driven image processing techniques holds immense potential for advancing our understanding of cardiac physiology and pathology.

In the future, my focus will be on conducting experiments aimed at expanding our current knowledge. The immediate objective is to demonstrate the capability of the single-cell device in detecting drug toxicity within the complex cellular environment. By exposing cardiomyocytes to various pharmaceutical agents, we seek to unravel intricate responses at the single-cell level,

highlighting the importance of analyzing drug effects with unprecedented precision. The significance of this thesis goes beyond the development of a new measurement tool. It offers valuable insights into the behavior of cardiac tissue and its reactions to external stimuli, thus contributing to our comprehension of cardiac physiology and pathology. Furthermore, the device's ability to discern variations in contractility during drug evaluations holds significant promise for drug toxicity testing. By facilitating precise monitoring of drug effects at the single-cell level, this technology has the potential to transform drug screening and development procedures, ultimately leading to the creation of safer and more effective pharmaceuticals.

Finally, the device presented in this thesis offers a remarkable opportunity to monitor the propagation of contraction through single-cell detection. By enabling the measurement of contractility at the level of individual cells, this technology opens new avenues for understanding the dynamics of contraction propagation within cardiac tissue. Looking ahead, future perspectives include further exploration of how contraction propagates through interconnected cardiomyocytes. By integrating advanced imaging techniques with the single-cell detection capability of the device, the sequential activation of individual cells during contraction can be investigated. This deeper understanding of contraction propagation patterns could yield insights into the coordination and synchronization of cardiac muscle activity. Additionally, the device's ability to precisely measure contractility at the single-cell level offers the potential for more targeted interventions in cardiac therapies. By identifying aberrant contraction patterns in specific cells or regions, clinicians may be able to develop tailored treatments to address cardiac dysfunction with greater precision and efficacy. Overall, the ability to monitor contraction propagation through single-cell detection represents a promising direction for future research in cardiac physiology and pathology. Through continued innovation and exploration, this technology has the potential to significantly advance our understanding of cardiac function and improve clinical outcomes for patients with heart-related conditions.

In this thesis, an innovative technology for the in vitro measurement of contractility in CMs monolayers was introduced, leveraging a micro-interferometric approach. Notably, the device can estimate various critical parameters such as frequency, shape, and amplitude of the contractile force generated by the cell culture. While the current architecture operates at the level of the whole cell culture, the concept can be translated to a smaller scale through proper device design,

achieving single-cell resolution. This advancement will aid in distinguishing the diverse contributions of individual cells to the overall tissue contraction. Additionally, the concept can be extended to various scenarios where biological tissues exert forces translatable into measurable displacements.

6 References

(1) Tortora, G. J., & Nielsen, M. *Principles of Human Anatomy*, 15th Editi.; Wiley, 2020.

(2) Hall, J. E. (John E.; Guyton, A. C. *Guyton and Hall Textbook of Medical Physiology* , 12th ed.; Saunders/Elsevier: Philadelphia, PA, 2011.

(3) Silverthorn, D. U.; Ober, W. C.; Garrison, C. W.; Silverthorn, A. C.; Johnson, B. R. *Human Physiology: An Integrated Approach*; Pearson Education Indianapolis, IN, 2013; Vol. 3.

(4) Navarrete, E. G.; Liang, P.; Lan, F.; Sanchez-Freire, V.; Simmons, C.; Gong, T.; Sharma, A.; Burridge, P. W.; Patlolla, B.; Lee, A. S.; Wu, H.; Beygui, R. E.; Wu, S. M.; Robbins, R. C.; Bers, D. M.; Wu, J. C. Screening Drug-Induced Arrhythmia [Corrected] Using Human Induced Pluripotent Stem Cell-Derived Cardiomyocytes and Low-Impedance Microelectrode Arrays. *Circulation* **2013**, *128* (11 Suppl 1), S3-13. https://doi.org/10.1161/CIRCULATIONAHA.112.000570.

(5) Forbes, M. S.; Sperelakis, N. Intercalated Discs of Mammalian Heart: A Review of Structure and Function. *Tissue Cell* **1985**, *17* (5), 605–648. https://doi.org/10.1016/0040-8166(85)90001-1.

(6) HUXLEY, A. F.; NIEDERGERKE, R. Structural Changes in Muscle during Contraction; Interference Microscopy of Living Muscle Fibres. *Nature* **1954**, *173* (4412), 971–973. https://doi.org/10.1038/173971a0.

(7) Mangoni, M. E.; Nargeot, J. Genesis and Regulation of the Heart Automaticity. *Physiol Rev* **2008**, *88* (3), 919–982. https://doi.org/10.1152/physrev.00018.2007.

(8) Souders, C. A.; Bowers, S. L. K.; Baudino, T. A. Cardiac Fibroblast: The Renaissance Cell. *Circ Res* **2009**, *105* (12), 1164–1176. https://doi.org/10.1161/CIRCRESAHA.109.209809.

(9) Roberts, N. K.; Castleman, K. R. Morphology of the Atrioventricular Node, Bundle and Proximal Bundle Branches: A Study Employing Computerized Reconstruction. *Anat Rec* **1979**, *195* (4), 699–706. https://doi.org/10.1002/ar.1091950409.

(10) Bers, D. M. Cardiac Excitation–Contraction Coupling. *Nature* **2002**, *415* (6868), 198–205. https://doi.org/10.1038/415198a.

(11) Bers, D. M. *No TitleExcitation-Contraction Coupling and Cardiac Contractile Force*; Springer Dordrecht, 2001. https://doi.org/https://doi.org/10.1007/978-94-010-0658-3.

(12) Vatta, M.; Faulkner, G. Cytoskeletal Basis of Ion Channel Function in Cardiac Muscle. *Future Cardiol* **2006**, *2* (4), 467–476. https://doi.org/10.2217/14796678.2.4.467.

(13) Rossi, D.; Pierantozzi, E.; Amadsun, D. O.; Buonocore, S.; Rubino, E. M.; Sorrentino, V. The Sarcoplasmic Reticulum of Skeletal Muscle Cells: A Labyrinth of Membrane Contact Sites. *Biomolecules* **2022**, *12* (4). https://doi.org/10.3390/biom12040488.

(14) Rossi, D.; Barone, V.; Giacomello, E.; Cusimano, V.; Sorrentino, V. The Sarcoplasmic Reticulum: An Organized Patchwork of Specialized Domains. *Traffic* **2008**, *9* (7), 1044–1049. https://doi.org/10.1111/j.1600-0854.2008.00717.x.

(15) Crocini, C.; Gotthardt, M. Cardiac Sarcomere Mechanics in Health and Disease. *Biophys Rev* **2021**, *13* (5), 637–652. https://doi.org/10.1007/s12551-021-00840-7.

(16) HUXLEY, H.; HANSON, J. Changes in the Cross-Striations of Muscle during Contraction and Stretch and Their Structural Interpretation. *Nature* **1954**, *173* (4412), 973–976. https://doi.org/10.1038/173973a0.

(17) (Joyce) Chen, C. -n.; Thompson, L. D. V; Snow, L. A. Chapter 1 - Muscle Structure and Function; Placzek, J. D., Boyce, D. A. B. T.-O. P. T. S. (Third E., Eds.; Elsevier, 2017; pp 1–9. https://doi.org/https://doi.org/10.1016/B978-0-323-28683-1.00001-1.

(18) Severs, N. J. Gap Junction Remodeling and Cardiac Arrhythmogenesis: Cause or Coincidence? *J Cell Mol Med* **2001**, *5* (4), 355–366. https://doi.org/10.1111/j.1582-4934.2001.tb00170.x.

(19) Forte, E. Visualization and Targeting of the Cardiac Conduction System. *Nature Cardiovascular Research* **2022**, *1* (9), 792. https://doi.org/10.1038/s44161-022-00135-4.

(20) van Meer, B. J.; Krotenberg, A.; Sala, L.; Davis, R. P.; Eschenhagen, T.; Denning, C.; Tertoolen, L. G. J.; Mummery, C. L. Simultaneous Measurement of Excitation-Contraction Coupling Parameters Identifies Mechanisms Underlying Contractile Responses of HiPSC-Derived Cardiomyocytes. *Nat Commun* **2019**, *10* (1), 4325. https://doi.org/10.1038/s41467-019-12354-8.

(21) Dobrzynski, H.; Anderson, R. H.; Atkinson, A.; Borbas, Z.; D'Souza, A.; Fraser, J. F.; Inada, S.; Logantha, S. J. R. J.; Monfredi, O.; Morris, G. M.; Moorman, A. F. M.; Nikolaidou, T.; Schneider, H.; Szuts, V.; Temple, I. P.; Yanni, J.; Boyett, M. R. Structure, Function and Clinical Relevance of the Cardiac Conduction System, Including the Atrioventricular Ring and Outflow Tract Tissues. *Pharmacol Ther* **2013**, *139* (2), 260–288. https://doi.org/https://doi.org/10.1016/j.pharmthera.2013.04.010.

(22) Garcia-Bustos, V.; Sebastian, R.; Izquierdo, M.; Molina, P.; Chorro, F. J.; Ruiz-Sauri, A. A Quantitative Structural and Morphometric Analysis of the Purkinje Network and the Purkinje–Myocardial Junctions in Pig Hearts. *J Anat* **2017**, *230* (5), 664–678. https://doi.org/https://doi.org/10.1111/joa.12594.

(23) Sala, L.; van Meer, B. J.; Tertoolen, L. G. J.; Bakkers, J.; Bellin, M.; Davis, R. P.; Denning, C.; Dieben, M. A. E.; Eschenhagen, T.; Giacomelli, E.; Grandela, C.; Hansen, A.; Holman, E. R.; Jongbloed, M. R. M.; Kamel, S. M.; Koopman, C. D.; Lachaud, Q.; Mannhardt, I.; Mol, M. P. H.; Mosqueira, D.; Orlova, V. V; Passier, R.; Ribeiro, M. C.; Saleem, U.; Smith, G. L.; Burton, F. L.; Mummery, C. L. MUSCLEMOTION. *Circ Res* **2018**, *122* (3), e5–e16. https://doi.org/10.1161/CIRCRESAHA.117.312067.

(24) Ahmed, R. E.; Anzai, T.; Chanthra, N.; Uosaki, H. A Brief Review of Current Maturation Methods for Human Induced Pluripotent Stem Cells-Derived Cardiomyocytes. *Front Cell Dev Biol* **2020**, *8*. https://doi.org/10.3389/fcell.2020.00178.

(25) Hirt, M. N.; Hansen, A.; Eschenhagen, T. Cardiac Tissue Engineering. *Circ Res* **2014**, *114* (2), 354–367. https://doi.org/10.1161/CIRCRESAHA.114.300522.

(26) Burridge, P. W.; Li, Y. F.; Matsa, E.; Wu, H.; Ong, S.-G.; Sharma, A.; Holmström, A.; Chang, A. C.; Coronado, M. J.; Ebert, A. D.; Knowles, J. W.; Telli, M. L.; Witteles, R. M.; Blau, H. M.; Bernstein, D.; Altman, R. B.; Wu, J. C. Human Induced Pluripotent Stem Cell-Derived Cardiomyocytes Recapitulate the Predilection of Breast Cancer Patients to Doxorubicin-Induced Cardiotoxicity. *Nat Med* **2016**, *22* (5), 547–556. https://doi.org/10.1038/nm.4087.

(27) Magdy, T.; Schuldt, A. J. T.; Wu, J. C.; Bernstein, D.; Burridge, P. W. Human Induced Pluripotent Stem Cell (HiPSC)-Derived Cells to Assess Drug Cardiotoxicity: Opportunities and Problems. *Annu Rev Pharmacol Toxicol* **2018**, *58* (1), 83–103. https://doi.org/10.1146/annurev-pharmtox-010617-053110.

(28) Denning, C.; Borgdorff, V.; Crutchley, J.; Firth, K. S. A.; George, V.; Kalra, S.; Kondrashov, A.; Hoang, M. D.; Mosqueira, D.; Patel, A.; Prodanov, L.; Rajamohan, D.; Skarnes, W. C.; Smith, J. G. W.; Young, L. E. Cardiomyocytes from Human Pluripotent Stem Cells: From Laboratory Curiosity to Industrial Biomedical Platform. *Biochimica et Biophysica Acta (BBA) - Molecular Cell Research* **2016**, *1863* (7, Part B), 1728–1748. https://doi.org/https://doi.org/10.1016/j.bbamcr.2015.10.014.

(29) Lalonde, R. L.; Kowalski, K. G.; Hutmacher, M. M.; Ewy, W.; Nichols, D. J.; Milligan, P. A.; Corrigan, B. W.; Lockwood, P. A.; Marshall, S. A.; Benincosa, L. J.; Tensfeldt, T. G.; Parivar, K.; Amantea, M.; Glue, P.; Koide, H.; Miller, R. Model-Based Drug Development. *Clin Pharmacol Ther* **2007**, *82* (1), 21–32. https://doi.org/https://doi.org/10.1038/sj.clpt.6100235.

(30) Drews, J.; Ryser, S. Drug Development: The Role of Innovation in Drug Development. *Nat Biotechnol* **1997**, *15* (13), 1318–1319. https://doi.org/10.1038/nbt1297-1318.

(31) Iachetta, G.; Colistra, N.; Melle, G.; Deleye, L.; Tantussi, F.; De Angelis, F.; Dipalo, M. Improving Reliability and Reducing Costs of Cardiotoxicity Assessments Using Laser-Induced Cell Poration on Microelectrode Arrays. *Toxicol Appl Pharmacol* **2021**, *418*, 115480. https://doi.org/10.1016/j.taap.2021.115480.

(32) Iachetta, G.; Melle, G.; Colistra, N.; Tantussi, F.; De Angelis, F.; Dipalo, M. Long-Term in Vitro Recording of Cardiac Action Potentials on Microelectrode Arrays for Chronic Cardiotoxicity Assessment. *Arch Toxicol* **2023**, *97* (2), 509–522. https://doi.org/10.1007/s00204-022-03422-y.

(33) Melle, G.; Bruno, G.; Maccaferri, N.; Iachetta, G.; Colistra, N.; Barbaglia, A.; Dipalo, M.; De Angelis, F. Intracellular Recording of Human Cardiac Action Potentials on Market-Available Multielectrode Array Platforms. *Front Bioeng Biotechnol* **2020**, *8*, 66. https://doi.org/10.3389/fbioe.2020.00066.

(34) Dipalo, M.; Melle, G.; Lovato, L.; Jacassi, A.; Santoro, F.; Caprettini, V.; Schirato, A.; Alabastri, A.; Garoli, D.; Bruno, G.; Tantussi, F.; De Angelis, F. Plasmonic Meta-Electrodes Allow Intracellular Recordings at Network Level on High-Density CMOS-Multi-Electrode Arrays. *Nat Nanotechnol* **2018**, *13* (10), 965–971. https://doi.org/10.1038/s41565-018-0222-z.

(35) Dipalo, M.; Rastogi, S. K.; Matino, L.; Garg, R.; Bliley, J.; Iachetta, G.; Melle, G.; Shrestha, R.; Shen, S.; Santoro, F.; Feinberg, A. W.; Barbaglia, A.; Cohen-Karni, T.; De Angelis, F. Intracellular Action Potential Recordings from Cardiomyocytes by Ultrafast Pulsed Laser Irradiation of Fuzzy Graphene Microelectrodes. *Sci Adv* **2023**, *7* (15), eabd5175. https://doi.org/10.1126/sciadv.abd5175.

(36) Bruno, G.; Melle, G.; Barbaglia, A.; Iachetta, G.; Melikov, R.; Perrone, M.; Dipalo, M.; De Angelis, F. All-Optical and Label-Free Stimulation of Action Potentials in Neurons and Cardiomyocytes by Plasmonic Porous Metamaterials. *Advanced Science* **2021**, *8* (21), 2100627. https://doi.org/https://doi.org/10.1002/advs.202100627.

(37) Ronaldson-Bouchard, K.; Vunjak-Novakovic, G. Organs-on-a-Chip: A Fast Track for Engineered Human Tissues in Drug Development. *Cell Stem Cell* **2018**, *22* (3), 310–324. https://doi.org/10.1016/j.stem.2018.02.011.

(38) Mathur, A.; Loskill, P.; Shao, K.; Huebsch, N.; Hong, S.; Marcus, S. G.; Marks, N.; Mandegar, M.; Conklin, B. R.; Lee, L. P.; Healy, K. E. Human IPSC-Based Cardiac Microphysiological System for Drug Screening Applications. *Sci Rep* **2015**, *5*, 8883. https://doi.org/10.1038/srep08883.

(39) Oyunbaatar, N.-E.; Lee, D.-H.; Patil, S. J.; Kim, E.-S.; Lee, D.-W. Biomechanical Characterization of Cardiomyocyte Using PDMS Pillar with Microgrooves. *Sensors* **2016**, *16* (8). https://doi.org/10.3390/s16081258.

(40) Sabass, B.; Gardel, M. L.; Waterman, C. M.; Schwarz, U. S. High Resolution Traction Force Microscopy Based on Experimental and Computational Advances. *Biophys J* **2008**, *94* (1), 207–220. https://doi.org/10.1529/biophysj.107.113670.

(41) Ribeiro, M. C.; Tertoolen, L. G.; Guadix, J. A.; Bellin, M.; Kosmidis, G.; D'Aniello, C.; Monshouwer-Kloots, J.; Goumans, M.-J.; Wang, Y.; Feinberg, A. W.; Mummery, C. L.; Passier, R. Functional Maturation of Human Pluripotent Stem Cell Derived Cardiomyocytes

in Vitro – Correlation between Contraction Force and Electrophysiology. *Biomaterials* **2015**, *51*, 138–150. https://doi.org/https://doi.org/10.1016/j.biomaterials.2015.01.067.

(42) Xi, B.; Wang, T.; Li, N.; Ouyang, W.; Zhang, W.; Wu, J.; Xu, X.; Wang, X.; Abassi, Y. A. Functional Cardiotoxicity Profiling and Screening Using the XCELLigence RTCA Cardio System. *JALA: Journal of the Association for Laboratory Automation* **2011**, *16* (6), 415–421. https://doi.org/10.1016/j.jala.2011.09.002.

(43) Dou, W.; Zhao, Q.; Malhi, M.; Liu, X.; Zhang, Z.; Wang, L.; Masse, S.; Nanthakumar, K.; Hamilton, R.; Maynes, J. T.; Sun, Y. Label-Free Conduction Velocity Mapping and Gap Junction Assessment of Functional IPSC-Cardiomyocyte Monolayers. *Biosens Bioelectron* **2020**, *167*, 112468. https://doi.org/https://doi.org/10.1016/j.bios.2020.112468.

(44) Ribeiro, A. J. S.; Ang, Y.-S.; Fu, J.-D.; Rivas, R. N.; Mohamed, T. M. A.; Higgs, G. C.; Srivastava, D.; Pruitt, B. L. Contractility of Single Cardiomyocytes Differentiated from Pluripotent Stem Cells Depends on Physiological Shape and Substrate Stiffness. *Proc Natl Acad Sci U S A* **2015**, *112* (41), 12705–12710. https://doi.org/10.1073/pnas.1508073112.

(45) Pioner, J. M.; Racca, A. W.; Klaiman, J. M.; Yang, K.-C.; Guan, X.; Pabon, L.; Muskheli, V.; Zaunbrecher, R.; Macadangdang, J.; Jeong, M. Y.; Mack, D. L.; Childers, M. K.; Kim, D.-H.; Tesi, C.; Poggesi, C.; Murry, C. E.; Regnier, M. Isolation and Mechanical Measurements of Myofibrils from Human Induced Pluripotent Stem Cell-Derived Cardiomyocytes. *Stem Cell Reports* **2016**, *6* (6), 885–896. https://doi.org/https://doi.org/10.1016/j.stemcr.2016.04.006.

(46) Haase, K.; Pelling, A. E. Investigating Cell Mechanics with Atomic Force Microscopy. *J R Soc Interface* **2015**, *12* (104), 20140970. https://doi.org/10.1098/rsif.2014.0970.

(47) Zanetti, M.; Andolfi, L.; Taylor, M. R. G.; Mestroni, L.; Lazzarino, M. AFM Macro-Probes to Investigate Whole 3D Cardiac Spheroids. *Micro and Nano Engineering* **2022**, *15*, 100134. https://doi.org/https://doi.org/10.1016/j.mne.2022.100134.

(48) Liu, Y.; Feng, J.; Shi, L.; Niu, R.; Sun, Q.; Liu, H.; Li, J.; Guo, J.; Zhu, J.; Han, D. In Situ Mechanical Analysis of Cardiomyocytes at Nano Scales. *Nanoscale* **2012**, *4* (1), 99–102. https://doi.org/10.1039/C1NR11303H.

(49) Domke, J.; Parak, W. J.; George, M.; Gaub, H. E.; Radmacher, M. Mapping the Mechanical Pulse of Single Cardiomyocytes with the Atomic Force Microscope. *European Biophysics Journal* **1999**, *28* (3), 179–186. https://doi.org/10.1007/s002490050198.

(50) Janssen, P. M. L. Myocardial Contraction-Relaxation Coupling. *American Journal of Physiology-Heart and Circulatory Physiology* **2010**, *299* (6), H1741–H1749. https://doi.org/10.1152/ajpheart.00759.2010.

(51) Huebsch, N.; Loskill, P.; Mandegar, M. A.; Marks, N. C.; Sheehan, A. S.; Ma, Z.; Mathur, A.; Nguyen, T. N.; Yoo, J. C.; Judge, L. M.; Spencer, C. I.; Chukka, A. C.; Russell, C. R.; So, P.-L.; Conklin, B. R.; Healy, K. E. Automated Video-Based Analysis of Contractility and Calcium Flux in Human-Induced Pluripotent Stem Cell-Derived Cardiomyocytes

Cultured over Different Spatial Scales. *Tissue Eng Part C Methods* **2015**, *21* (5), 467–479. https://doi.org/10.1089/ten.TEC.2014.0283.

(52) Ahola, A.; Pradhapan, P.; Laurila, E.; Aalto-Setälä, K.; Hyttinen, J. Motion Analysis Method for Determining Cardiomyocyte Beating Properties Based on Digital Image Correlation and Templates. In *Computing in Cardiology 2014*; 2014; pp 1137–1140.

(53) Dou, W.; Malhi, M.; Zhao, Q.; Wang, L.; Huang, Z.; Law, J.; Liu, N.; Simmons, C. A.; Maynes, J. T.; Sun, Y. Microengineered Platforms for Characterizing the Contractile Function of in Vitro Cardiac Models. *Microsyst Nanoeng* **2022**, *8* (1), 26. https://doi.org/10.1038/s41378-021-00344-0.

(54) Ronaldson-Bouchard, K.; Ma, S. P.; Yeager, K.; Chen, T.; Song, L.; Sirabella, D.; Morikawa, K.; Teles, D.; Yazawa, M.; Vunjak-Novakovic, G. Advanced Maturation of Human Cardiac Tissue Grown from Pluripotent Stem Cells. *Nature* **2018**, *556* (7700), 239–243. https://doi.org/10.1038/s41586-018-0016-3.

(55) Soares, C. P.; Midlej, V.; Oliveira, M. E. W. de; Benchimol, M.; Costa, M. L.; Mermelstein, C. 2D and 3D-Organized Cardiac Cells Shows Differences in Cellular Morphology, Adhesion Junctions, Presence of Myofibrils and Protein Expression. *PLoS One* **2012**, *7* (5), e38147. https://doi.org/10.1371/journal.pone.0038147.

(56) Nguemo, F.; Šaric, T.; Pfannkuche, K.; Watzele, M.; Reppel, M.; Hescheler, J. In Vitro Model for Assessing Arrhythmogenic Properties of Drugs Based on High-Resolution Impedance Measurements. *Cellular Physiology and Biochemistry* **2012**, *29* (5–6), 819–832. https://doi.org/10.1159/000188069.

(57) Magar, H. S.; Hassan, R. Y. A.; Mulchandani, A. Electrochemical Impedance Spectroscopy (EIS): Principles, Construction, and Biosensing Applications. *Sensors (Basel)* **2021**, *21* (19). https://doi.org/10.3390/s21196578.

(58) Giaever, I.; Keese, C. R. A Morphological Biosensor for Mammalian Cells. *Nature* **1993**, *366* (6455), 591–592. https://doi.org/10.1038/366591a0.

(59) Zhang, X.; Wang, W.; Li, F.; Voiculescu, I. Stretchable Impedance Sensor for Mammalian Cell Proliferation Measurements. *Lab Chip* **2017**, *17* (12), 2054–2066. https://doi.org/10.1039/C7LC00375G.

(60) Wang, X.; Wang, L.; Dou, W.; Huang, Z.; Zhao, Q.; Malhi, M.; Maynes, J. T.; Sun, Y. Electrical Impedance-Based Contractile Stress Measurement of Human IPSC-Cardiomyocytes. *Biosens Bioelectron* **2020**, *166*, 112399. https://doi.org/https://doi.org/10.1016/j.bios.2020.112399.

(61) Scott, C. W.; Zhang, X.; Abi-Gerges, N.; Lamore, S. D.; Abassi, Y. A.; Peters, M. F. An Impedance-Based Cellular Assay Using Human IPSC-Derived Cardiomyocytes to Quantify Modulators of Cardiac Contractility. *Toxicological Sciences* **2014**, *142* (2), 331–338. https://doi.org/10.1093/toxsci/kfu186.

(62) Goßmann, M.; Frotscher, R.; Linder, P.; Neumann, S.; Bayer, R.; Epple, M.; Staat, M.; (Temiz) Artmann, A.; Artmann, G. M. Mechano-Pharmacological Characterization of Cardiomyocytes Derived from Human Induced Pluripotent Stem Cells. *Cellular Physiology and Biochemistry* **2016**, *38* (3), 1182–1198. https://doi.org/10.1159/000443124.

(63) Mouro, J.; Pinto, R.; Paoletti, P.; Tiribilli, B. Microcantilever: Dynamical Response for Mass Sensing and Fluid Characterization. *Sensors* **2020**, *21* (1), 115. https://doi.org/10.3390/s21010115.

(64) Kim, D.-S.; Jeong, Y.-J.; Lee, B.-K.; Shanmugasundaram, A.; Lee, D.-W. Piezoresistive Sensor-Integrated PDMS Cantilever: A New Class of Device for Measuring the Drug-Induced Changes in the Mechanical Activity of Cardiomyocytes. *Sens Actuators B Chem* **2017**, *240* (C), 566–572. https://doi.org/10.1016/j.snb.2016.08.167.

(65) Zhao, Z.; Jeong, Y.-J.; Oyunbaatar, N.-E.; Pujari, R. B.; Kanade, P. P.; Kim, E.-S.; Lee, B.-K.; Lee, D.-W. Simultaneous Measurement of Contraction Forces and Field Potentials of Cardiomyocytes Subjected to Ion Channel Inhibitors. *Sens Actuators B Chem* **2022**, *358*, 131495. https://doi.org/https://doi.org/10.1016/j.snb.2022.131495.

(66) Ohya, T.; Ohtomo, H.; Kikuchi, T.; Sasaki, D.; Kawamura, Y.; Matsuura, K.; Shimizu, T.; Fukuda, K.; Someya, T.; Umezu, S. Simultaneous Measurement of Contractile Force and Field Potential of Dynamically Beating Human IPS Cell-Derived Cardiac Cell Sheet-Tissue with Flexible Electronics. *Lab Chip* **2021**, *21* (20), 3899–3909. https://doi.org/10.1039/D1LC00411E.

(67) Dou, W.; Daoud, A.; Chen, X.; Wang, T.; Malhi, M.; Gong, Z.; Mirshafiei, F.; Zhu, M.; Shan, G.; Huang, X.; Maynes, J. T.; Sun, Y. Ultrathin and Flexible Bioelectronic Arrays for Functional Measurement of IPSC-Cardiomyocytes under Cardiotropic Drug Administration and Controlled Microenvironments. *Nano Lett* **2023**, *23* (6), 2321–2331. https://doi.org/10.1021/acs.nanolett.3c00017.

(68) Boudou, T.; Legant, W. R.; Mu, A.; Borochin, M. A.; Thavandiran, N.; Radisic, M.; Zandstra, P. W.; Epstein, J. A.; Margulies, K. B.; Chen, C. S. A Microfabricated Platform to Measure and Manipulate the Mechanics of Engineered Cardiac Microtissues. *Tissue Eng Part A* **2012**, *18* (9–10), 910–919. https://doi.org/10.1089/ten.tea.2011.0341.

(69) Dai, Y.; Oyunbaatar, N.-E.; Lee, B.-K.; Kim, E.-S.; Lee, D.-W. Spiral-Shaped SU-8 Cantilevers for Monitoring Mechanical Response of Cardiomyocytes Treated with Cardiac Drugs. *Sens Actuators B Chem* **2018**, *255*, 3391–3399. https://doi.org/https://doi.org/10.1016/j.snb.2017.09.168.

(70) Kim, J. Y.; Choi, Y.-S.; Lee, B.-K.; Lee, D.-W. Surface-Patterned SU-8 Cantilever Arrays for Preliminary Screening of Cardiac Toxicity. *Biosens Bioelectron* **2016**, *80*, 456–462. https://doi.org/https://doi.org/10.1016/j.bios.2016.01.089.

(71) Zhao, Y.; Rafatian, N.; Wang, E. Y.; Wu, Q.; Lai, B. F. L.; Lu, R. X.; Savoji, H.; Radisic, M. Towards Chamber Specific Heart-on-a-Chip for Drug Testing Applications. *Adv Drug Deliv Rev* **2020**, *165–166*, 60–76. https://doi.org/10.1016/j.addr.2019.12.002.

(72) Tiburcy, M.; Hudson, J. E.; Balfanz, P.; Schlick, S.; Meyer, T.; Chang Liao, M.-L.; Levent, E.; Raad, F.; Zeidler, S.; Wingender, E.; Riegler, J.; Wang, M.; Gold, J. D.; Kehat, I.; Wettwer, E.; Ravens, U.; Dierickx, P.; van Laake, L. W.; Goumans, M. J.; Khadjeh, S.; Toischer, K.; Hasenfuss, G.; Couture, L. A.; Unger, A.; Linke, W. A.; Araki, T.; Neel, B.; Keller, G.; Gepstein, L.; Wu, J. C.; Zimmermann, W.-H. Defined Engineered Human Myocardium With Advanced Maturation for Applications in Heart Failure Modeling and Repair. *Circulation* **2017**, *135* (19), 1832–1847. https://doi.org/10.1161/CIRCULATIONAHA.116.024145.

(73) Ingber, D. E. Human Organs-on-Chips for Disease Modelling, Drug Development and Personalized Medicine. *Nat Rev Genet* **2022**, *23* (8), 467–491. https://doi.org/10.1038/s41576-022-00466-9.

(74) Ye, K. Y.; Black, L. D. 3rd. Strategies for Tissue Engineering Cardiac Constructs to Affect Functional Repair Following Myocardial Infarction. *J Cardiovasc Transl Res* **2011**, *4* (5), 575–591. https://doi.org/10.1007/s12265-011-9303-1.

(75) Benjamin, E. J.; Muntner, P.; Alonso, A.; Bittencourt, M. S.; Callaway, C. W.; Carson, A. P.; Chamberlain, A. M.; Chang, A. R.; Cheng, S.; Das, S. R.; Delling, F. N.; Djousse, L.; Elkind, M. S. V; Ferguson, J. F.; Fornage, M.; Jordan, L. C.; Khan, S. S.; Kissela, B. M.; Knutson, K. L.; Kwan, T. W.; Lackland, D. T.; Lewis, T. T.; Lichtman, J. H.; Longenecker, C. T.; Loop, M. S.; Lutsey, P. L.; Martin, S. S.; Matsushita, K.; Moran, A. E.; Mussolino, M. E.; O'Flaherty, M.; Pandey, A.; Perak, A. M.; Rosamond, W. D.; Roth, G. A.; Sampson, U. K. A.; Satou, G. M.; Schroeder, E. B.; Shah, S. H.; Spartano, N. L.; Stokes, A.; Tirschwell, D. L.; Tsao, C. W.; Turakhia, M. P.; VanWagner, L. B.; Wilkins, J. T.; Wong, S. S.; Virani, S. S.; null, null. Heart Disease and Stroke Statistics—2019 Update: A Report From the American Heart Association. *Circulation* **2019**, *139* (10), e56–e528. https://doi.org/10.1161/CIR.0000000000000659.

(76) Yancy, C. W.; Jessup, M.; Bozkurt, B.; Butler, J.; Casey, D. E. J.; Colvin, M. M.; Drazner, M. H.; Filippatos, G. S.; Fonarow, G. C.; Givertz, M. M.; Hollenberg, S. M.; Lindenfeld, J.; Masoudi, F. A.; McBride, P. E.; Peterson, P. N.; Stevenson, L. W.; Westlake, C. 2017 ACC/AHA/HFSA Focused Update of the 2013 ACCF/AHA Guideline for the Management of Heart Failure: A Report of the American College of Cardiology/American Heart Association Task Force on Clinical Practice Guidelines and the Heart Failure Society of Ame. *Circulation* **2017**, *136* (6), e137–e161. https://doi.org/10.1161/CIR.0000000000000509.

(77) Houser, S. R.; Margulies, K. B. Is Depressed Myocyte Contractility Centrally Involved in Heart Failure? *Circ Res* **2003**, *92* (4), 350–358. https://doi.org/10.1161/01.RES.0000060027.40275.A6.

(78) Reilly, L.; Munawar, S.; Zhang, J.; Crone, W. C.; Eckhardt, L. L. Challenges and Innovation: Disease Modeling Using Human-Induced Pluripotent Stem Cell-Derived Cardiomyocytes. *Front Cardiovasc Med* **2022**, *9*. https://doi.org/10.3389/fcvm.2022.966094.

(79) Davis, J.; Chouman, A.; Creech, J.; Monteiro da Rocha, A.; Ponce-Balbuena, D.; Jimenez Vazquez, E. N.; Nichols, R.; Lozhkin, A.; Madamanchi, N. R.; Campbell, K. F.; Herron, T. J. In Vitro Model of Ischemic Heart Failure Using Human Induced Pluripotent Stem Cell–Derived Cardiomyocytes. *JCI Insight* **2021**, *6* (10). https://doi.org/10.1172/jci.insight.134368.

(80) Zhu, K.; Bao, X.; Wang, Y.; Lu, T.; Zhang, L. Human Induced Pluripotent Stem Cell (HiPSC)-Derived Cardiomyocyte Modelling of Cardiovascular Diseases for Natural Compound Discovery. *Biomedicine & Pharmacotherapy* **2023**, *157*, 113970. https://doi.org/https://doi.org/10.1016/j.biopha.2022.113970.

(81) Ribeiro, A. J. S.; Guth, B. D.; Engwall, M.; Eldridge, S.; Foley, C. M.; Guo, L.; Gintant, G.; Koerner, J.; Parish, S. T.; Pierson, J. B.; Brock, M.; Chaudhary, K. W.; Kanda, Y.; Berridge, B. Considerations for an In Vitro, Cell-Based Testing Platform for Detection of Drug-Induced Inotropic Effects in Early Drug Development. Part 2: Designing and Fabricating Microsystems for Assaying Cardiac Contractility With Physiological Relevance Using Hu. *Front Pharmacol* **2019**, *10*, 934. https://doi.org/10.3389/fphar.2019.00934.

(82) Kim, D.-S.; Choi, Y. W.; Shanmugasundaram, A.; Jeong, Y.-J.; Park, J.; Oyunbaatar, N.-E.; Kim, E.-S.; Choi, M.; Lee, D.-W. Highly Durable Crack Sensor Integrated with Silicone Rubber Cantilever for Measuring Cardiac Contractility. *Nat Commun* **2020**, *11* (1), 535. https://doi.org/10.1038/s41467-019-14019-y.

(83) Dou, W.; Malhi, M.; Zhao, Q.; Wang, L.; Huang, Z.; Law, J.; Liu, N.; Simmons, C. A.; Maynes, J. T.; Sun, Y. Microengineered Platforms for Characterizing the Contractile Function of in Vitro Cardiac Models. *Microsyst Nanoeng* **2022**, *8* (1), 26. https://doi.org/10.1038/s41378-021-00344-0.

(84) Wei, X.; Zhuang, L.; Li, H.; He, C.; Wan, H.; Hu, N.; Wang, P. Advances in Multidimensional Cardiac Biosensing Technologies: From Electrophysiology to Mechanical Motion and Contractile Force. *Small* **2020**, *16*. https://doi.org/10.1002/smll.202005828.

(85) Liu, J.; Sun, N.; Bruce, M. A.; Wu, J. C.; Butte, M. J. Atomic Force Mechanobiology of Pluripotent Stem Cell-Derived Cardiomyocytes. *PLoS One* **2012**, *7* (5), e37559. https://doi.org/10.1371/journal.pone.0037559.

(86) Balashov, V. A.; Gorbunov, V. S.; Guria, K. G.; Agladze, K. I. Muscular Thin Films for Label-Free Mapping of Excitation Propagation in Cardiac Tissue. *Ann Biomed Eng* **2020**, *48* (10), 2425–2437. https://doi.org/10.1007/s10439-020-02513-0.

(87) Vahala, K. J. Optical Microcavities. *Nature* **2003**, *424* (6950), 839–846. https://doi.org/10.1038/nature01939.

(88) Schiller, S. Spectrometry with Frequency Combs. *Opt Lett* **2002**, *27* (9), 766–768. https://doi.org/10.1364/ol.27.000766.

(89) Barbaglia, A.; Dipalo, M.; Melle, G.; Iachetta, G.; Deleye, L.; Hubarevich, A.; Toma, A.; Tantussi, F.; De Angelis, F. Mirroring Action Potentials: Label-Free, Accurate, and Noninvasive Electrophysiological Recordings of Human-Derived Cardiomyocytes. *Advanced Materials* **2021**, *33* (7), 2004234. https://doi.org/https://doi.org/10.1002/adma.202004234.

(90) LeCun, Y.; Bengio, Y.; Hinton, G. Deep Learning. *Nature* **2015**, *521* (7553), 436–444. https://doi.org/10.1038/nature14539.

(91) Ruan, J.-L.; Tulloch, N. L.; Razumova, M. V; Saiget, M.; Muskheli, V.; Pabon, L.; Reinecke, H.; Regnier, M.; Murry, C. E. Mechanical Stress Conditioning and Electrical Stimulation Promote Contractility and Force Maturation of Induced Pluripotent Stem Cell-Derived Human Cardiac Tissue. *Circulation* **2016**, *134* (20), 1557–1567. https://doi.org/10.1161/CIRCULATIONAHA.114.014998.

(92) Swift, L. M.; Asfour, H.; Posnack, N. G.; Arutunyan, A.; Kay, M. W.; Sarvazyan, N. Properties of Blebbistatin for Cardiac Optical Mapping and Other Imaging Applications. *Pflugers Arch* **2012**, *464* (5), 503–512. https://doi.org/10.1007/s00424-012-1147-2.

(93) Fedorov, V.; Lozinsky, I.; Sosunov, E.; Anyukhovsky, E.; Rosen, M.; Balke, C.; Efimov, I. Application of Blebbistatin as an Excitation-Contraction Uncoupler for Electrophysiologic Study of Rat and Rabbit Hearts. *Heart rhythm : the official journal of the Heart Rhythm Society* **2007**, *4*, 619–626. https://doi.org/10.1016/j.hrthm.2006.12.047.

(94) Ventsel, E.; Krauthammer, T. *Thin Plates and Shells : Theory, Analysis, and Applications*; Marcel Dekker New York: New York SE -, 2001. https://doi.org/LK - https://worldcat.org/title/47168757.

(95) Maddux, G. E.; (U.S.), A. F. F. D. L. *Stress Analysis Manual*; Air Force Flight Dynamics Laboratory, Air Force Systems Command Wright-Patterson Air Force Base, Ohio: Wright-Patterson Air Force Base, Ohio SE -, 1970. https://doi.org/LK - https://worldcat.org/title/12959772.

(96) İmrak, C.; Gerdemeli, İ. An Exact Solution for the Deflection of a Clamped Rectangular Plate under Uniform Load. *Applied Mathematical Sciences (Ruse)* **2007**, *1*.

(97) Hakim, G.; Abramovich, H. Large Deflections of Thin-Walled Plates under Transverse Loading-Investigation of the Generated In-Plane Stresses. *Materials (Basel)* **2022**, *15* (4). https://doi.org/10.3390/ma15041577.

(98) Maddux, G. E.; Vorst, L. A.; Giessler, F.; Moritz, T. Stress Analysis Manual; 1969.

(99) Körner, A.; Mosqueira, M.; Hecker, M.; Ullrich, N. D. Substrate Stiffness Influences Structural and Functional Remodeling in Induced Pluripotent Stem Cell-Derived Cardiomyocytes. *Front Physiol* **2021**, *12*, 710619. https://doi.org/10.3389/fphys.2021.710619.

(100) Wright, P. T.; Tsui, S. F.; Francis, A. J.; MacLeod, K. T.; Marston, S. B. Approaches to High-Throughput Analysis of Cardiomyocyte Contractility. *Front Physiol* **2020**, *11*, 612. https://doi.org/10.3389/fphys.2020.00612.

(101) Paur, H.; Wright, P. T.; Sikkel, M. B.; Tranter, M. H.; Mansfield, C.; O'Gara, P.; Stuckey, D. J.; Nikolaev, V. O.; Diakonov, I.; Pannell, L.; Gong, H.; Sun, H.; Peters, N. S.; Petrou, M.; Zheng, Z.; Gorelik, J.; Lyon, A. R.; Harding, S. E. High Levels of Circulating Epinephrine Trigger Apical Cardiodepression in a B2-Adrenergic Receptor/Gi-Dependent Manner: A New Model of Takotsubo Cardiomyopathy. *Circulation* **2012**, *126* (6), 697–706. https://doi.org/10.1161/CIRCULATIONAHA.112.111591.

(102) Wright, P. T.; Bhogal, N. K.; Diakonov, I.; Pannell, L. M. K.; Perera, R. K.; Bork, N. I.; Schobesberger, S.; Lucarelli, C.; Faggian, G.; Alvarez-Laviada, A.; Zaccolo, M.; Kamp, T. J.; Balijepalli, R. C.; Lyon, A. R.; Harding, S. E.; Nikolaev, V. O.; Gorelik, J. Cardiomyocyte Membrane Structure and CAMP Compartmentation Produce Anatomical Variation in β(2)AR-CAMP Responsiveness in Murine Hearts. *Cell Rep* **2018**, *23* (2), 459–469. https://doi.org/10.1016/j.celrep.2018.03.053.

(103) Watkins, A. 24 - The Electrical Heart: Energy in Cardiac Health and Disease; Mayor, D., Micozzi, M. S. B. T.-E. M. E. and W., Eds.; Churchill Livingstone: Edinburgh, 2011; pp 305–317. https://doi.org/https://doi.org/10.1016/B978-0-7020-3571-5.00024-X.

(104) Campbell, K.; Calvo, C. J.; Mironov, S.; Herron, T.; Berenfeld, O.; Jalife, J. Spatial Gradients in Action Potential Duration Created by Regional Magnetofection of HERG Are a Substrate for Wavebreak and Turbulent Propagation in Cardiomyocyte Monolayers. *J Physiol* **2012**, *590* (24), 6363–6379. https://doi.org/https://doi.org/10.1113/jphysiol.2012.238758.

(105) Kuo, P.-L.; Lee, H.; Bray, M.-A.; Geisse, N. A.; Huang, Y.-T.; Adams, W. J.; Sheehy, S. P.; Parker, K. K. Myocyte Shape Regulates Lateral Registry of Sarcomeres and Contractility. *Am J Pathol* **2012**, *181* (6), 2030–2037. https://doi.org/https://doi.org/10.1016/j.ajpath.2012.08.045.

(106) Day, S. M.; Tardiff, J. C.; Ostap, E. M. Myosin Modulators: Emerging Approaches for the Treatment of Cardiomyopathies and Heart Failure. *J Clin Invest* **2022**, *132* (5). https://doi.org/10.1172/JCI148557.

(107) Yang, S.; Zhang, G. A Review of Interferometry for Geometric Measurement. *Meas Sci Technol* **2018**, *29* (10), 102001. https://doi.org/10.1088/1361-6501/aad732.

(108) Conor O'Mahony; Martin Hill; Magali Brunet; Russell Duane; Alan Mathewson. Characterization of Micromechanical Structures Using White-Light Interferometry. *Meas Sci Technol* **2003**, *14* (10), 1807. https://doi.org/10.1088/0957-0233/14/10/310.

(109) Lyshevski, S. E. *MEMS and NEMS: Systems, Devices, and Structures*; CRC press, 2018.

(110) Nolte, D. D. *Optical Interferometry for Biology and Medicine*; Springer Science & Business Media, 2011; Vol. 1.